A widespread electrical brain network encodes anxiety in health and depressive states

Dalton N. Hughes[3,*], Michael Hunter Klein[8,*], Kathryn Katsue Walder-Christensen[3,*], Gwenaëlle E. Thomas[3], Yael Grossman[2], Diana Waters[2], Anna Matthews[2], William E. Carson[10], Yassine Filali[7], Mariya Tsyglakova[6], Alexandra Fink[3], Neil M. Gallagher[3], Masiel Perez-Balaguer[2], Colleen A. McClung[6], Jean Mary Zarate[2], Rainbo C. Hultman[7], Stephen D. Mague[2], David E. Carlson[5,8,9,10,†], Kafui Dzirasa[1,2,3,4,†].

[1]Howard Hughes Medical Institute, Chevy Chase, Maryland 20815, USA; [2]Dept. of Psychiatry and Behavioral Sciences, [3]Dept. of Neurobiology, [4] Dept. of Neurosurgery, [5]Dept. of Biostatistics and Bioinformatics, Duke University Medical Center, Durham, North Carolina 27710, USA; [6]Department of Psychiatry, University of Pittsburgh Medical School, Pittsburgh, PA 15213; [7]Department of Molecular Physiology and Biophysics, Department of Psychiatry, University of Iowa, Iowa City, IA, 52242 USA; [8]Dept. of Electrical and Computer Engineering, [9]Dept. of Civil and Environmental Engineering, [10]Dept. of Biomedical Engineering, Duke University, Durham North Carolina 27708, USA.

*These co-first authors contributed equally

†Senior authors; Contributed equally

Keywords

Anxiety, brain networks, dynamics, limbic, depression, and stress.

Abstract

In rodents, anxiety is characterized by heightened vigilance during low-threat and uncertain situations. Though activity in the frontal cortex and limbic system is fundamental to supporting this internal state, the underlying network architecture that integrates activity across brain regions to encode anxiety across animals and paradigms remains unclear. Here, we utilize parallel electrical recordings in freely behaving mice, multiple translational paradigms known to induce anxiety, and machine learning to discover a multi-region network that encodes the anxious brain state. The network is composed of circuits widely implicated in anxiety behavior, it generalizes across many behavioral contexts that induce anxiety, and it fails to encode multiple behavioral contexts that do not. Strikingly, the activity of this network is also principally altered in two mouse models of depression. Thus, we establish a network-level process whereby the brain encodes anxiety in health and disease.

Anxiety is a mental state marked by heightened pressure, concern, or apprehension related to uncertain future circumstances [1]. The anxious state can be adaptive increasing the rate of survival, or it can become overly generalized and persistent in a manner that yields behavioral pathology that can lead to anxiety disorders. These disorders constitute the largest group of mental disorders in Western and high-income societies, with nearly 34% of U.S. adults directly impacted in their lifetime [1,2]. Strikingly, the prevalence of symptoms of anxiety disorders or other mental health disorders had increased during the height of the COVID-19 pandemic [3]. As such, it is imperative to discover the biological basis of the anxious brain state and to delineate how the brain encodes anxiety in the disordered state.

Non-invasive human imaging studies have demonstrated altered activity in multiple cortical and limbic brain regions, including the amygdala, prefrontal cortex, and hippocampus during heightened anxiety and synchronized activity between these regions and others at the millisecond-to-second timescales [4-7]. Human intracranial recordings have also demonstrated altered coherence in networks with some of these regions linked to higher trait anxiety [8], pointing towards the involvement of integrated multi-regional circuits in mediating the anxiety state.

A myriad of rodent studies have implicated homologous regions in mediating anxiety: the amygdala (Amy), ventral hippocampus (VHip), and subregions of the medial prefrontal cortex (mPFC). Pharmacological lesions and optogenetic inactivation studies have implicated the necessity of these brain regions for anxious behaviors [9,10]. Furthermore, precise circuit-level studies in rodent models have further delineated the role of these brain regions and their integrated circuits [11]. For example, millisecond-level coherence is observed in the mPFC, Amy and/or VHip during key aspects of anxiety-related behaviors [12-17], and optogenetic interrogation of projections involving these regions modulate anxiety-related behaviors [18-23]. Yet it remains to be clarified how these circuits reliably integrate across timescales (i.e., network-level stability) to selectively encode anxiety across animals and behavioral contexts (i.e., generalization) in healthy animals and in disease states.

Because local field potentials (LFPs) capture generalized patterns of neural activity that can be consistently sampled across subjects [24], we previously developed a machine learning technique called discriminative Cross-Spectral Factor Analysis-Nonnegative Matrix Factorization (dCSFA-NMF) to discover behaviorally relevant ensembles of LFP activity that synchronize at both the milliseconds and seconds timescale [i.e., electrical functional connectome ('electome') – networks]. An electome network can be composed by LFP oscillatory power from each brain area, millisecond-resolution coherence between oscillations from pairs of brain regions, and/or directional oscillations (an indication of information transfer between pairs of brain regions assessed using Granger causality testing), ranging from 1–56Hz. Moreover, dCSFA-NMF was designed to discover electome networks that encode behaviorally relevant internal states both within and across mice [25-27].

Here, we operationalized anxiety as an internal state characterized by increased behavioral inhibition in response to perceived threat, which can be assessed through measurable, test-dependent outcomes. These can include (but are not limited to) reduced exploration of exposed spaces, heightened physiological responses, hyperarousal, and vigilance patterns that facilitate the association of an ongoing threat with the context in which it is experienced. We then used dCSFA-NMF to discover a distinct electome network that selectively encodes anxiety induced by multiple contexts in healthy animals. The network was also activated in mouse models of stress disorders in a context that should otherwise not promote anxiety.

Results

Distributed electome networks encode a convergent anxious internal state

Forty-one male mice were implanted with multiwire electrodes to concurrently target mPFC [cingulate (Cg), prelimbic (PrL) and infralimbic (IL) cortex], Amy, VHip, nucleus accumbens (NAc), medial dorsal thalamus (MD), and ventral tegmental area (VTA; Fig. 1A, left). Following their recovery, we employed a two-stage approach to discover how distributed neural activity encodes an internal state for anxiety. First, we utilized a translational anxiogenic protocol based on treatment with the antidepressant fluoxetine (FLX). Acute administration of this class of agents is known to induce anxiety in humans, and it has been shown to increase behavioral inhibition in response to perceived threat in mice [28], versus a saline control condition (see also Supplemental Figure S1).

Second, we tested whether the electome networks learned for this paradigm also encoded the internal state induced by two paradigms characterized by increased behavioral inhibition with regards to exploration of exposed spaces: the elevated plus maze (EPM) and the bright open field (BOF). The amount of time a mouse spends within exposed regions of these assays (open arms in the EPM and center of the BOF) is widely used to infer anxious internal states. As mice with the highest anxiety-like behavior may never enter the exposed regions of these assays, we modeled anxiety as the internal state that was causally induced by the three paradigms (Fig. 1A, middle). All three paradigms heightened physiological responses in mice, as assessed via heart rate (T_6=2.6, T_7=2.4, T_8=2.9 and P=0.025, P=0.024, P=0.01 for the EPM, BOF, and FLX assays, respectively, using a one-tailed t-test; N=7-9 male mice per assay, see Fig. 1A, right), achieving our operational definition of anxiety. We trained our network model at one-second resolution to enable us to compare network activity to ongoing behaviors widely utilized to assess the anxiety state of mice [12,29]. This choice of one-second resolution balances temporal resolution and signal strength, as -longer windows would be expected to yield stronger signals with lower temporal resolution. The 41 implanted male mice were exposed to at least 1 of the 3 experimental paradigms; 17 mice were subjected to two paradigms (see also Supplemental Figure S2).

Our dCSFA-NMF model trained on the neural data acquired during the FLX paradigm successfully distinguished the low and high anxiety states in holdout subjects [saline and FLX treatment, respectively; Mann-Whitney Area under the curve of model performance (AUC) = 0.68 ± 0.01, where higher values indicated better model performance and 0.5 corresponds to chance; Fig. 1B, see also Supplemental Figure S3]; however, the model failed to distinguish low and high anxiety states when it was tested on data obtained from the other two paradigms (AUC = 0.49 ± 0.01 and 0.44 ± 0.01 for EPM and BOF, respectively). We also found that dCSFA-NMF models trained on the EPM or BOF assay similarly failed to distinguish the low and high anxiety states of the FLX assay. These analyses employed four-fold cross-validation with 3-7 holdout mice within assay per fold, and 9-26 holdout mice between assays per fold. A full discussion of the dCSFA-NMF model training procedure, hyperparameter selection, rigorous validation strategies can be found in the Methods section.

After failing to discover a generalized internal state for anxiety solely using training data from one paradigm, we took inspiration from multi-task learning [30] and adapted dCSFA-NMF for training on multiple assays jointly (Fig. 1C, see Supplemental Fig. S4). Specifically, the multi-assay dCSFA-NMF model utilized training data from all three contexts (FLX, EPM, BOF) to discover an electome network that was shared between them. Though we successfully discovered such a shared electome network, we also found that small permutations of the animal assignments between training and validation data groups yielded electome networks composed of different LFP spectral features (Fig. 1D) while remaining predictive of the high vs. low anxiety states.

To address this lack of stability, we developed and employed a cosine similarity-based metric for evaluating network stability across multiple training permutations. For this metric, a low cosine distance

reflects greater electome network consistency. We then systematically increased the number of supervised networks in our dCSFA-NMF model, utilizing all supervised networks in a joint prediction logistic regression framework, and quantified the stability of the resultant electome networks. With this approach, we found that a model trained with three supervised electome networks optimally balanced simplicity and electome network stability across multiple runs as evaluated on reshuffled and split training data (Supplemental Figure S5). For this multi-network model, higher activity was mapped to the high anxiety contexts across all three assays. This multi-network model also encoded the high anxiety context across all three assays in 20 newly implanted C57 mice that had not been used to train the model (AUC = 0.59 ± 0.04, 0.76 ± 0.03, and 0.84 ± 0.03 for FLX, EPM, and BOF, respectively; Fig. 1E). Although many individual brain regions/pairs of regions independently encoded two of the paradigms, no pairs encoded the anxiety state shared by all three paradigms (Fig. 1F, see also Supplemental Figure S6). Thus, our findings argued that the convergent anxiety brain state was encoded at the multi-region level. As expected, increasing the window length increases classifier discrimination (see Supplemental Figure S7).

Two electome networks independently encode the anxious internal state

The three supervised networks that jointly predicted the anxiety state contributed 26%, 73%, and 1% of the joint logistic regression model prediction probability, averaged across assays (heretofore referred to as Electome Networks 1, 2 and 3, respectively; see Fig. 2D). Electome Network 1 was comprised of prominent beta (14–30Hz) and gamma oscillations (30–55Hz) that led from VTA, amygdala, and medial dorsal thalamus, and converged in infralimbic cortex and nucleus accumbens. Electome Network 2 was comprised of prominent beta and gamma oscillations that led from prelimbic cortex, relayed through medial dorsal thalamus, and converged in the amygdala. Electome Network 3 was represented by synchronized theta oscillations (4–11Hz) across many of the regions we probed (Fig. 2A-C, see also Supplemental Figures S8-10). Thus, the three electome networks were each represented by distinct ensembles of LFP activity.

Importantly, the electome networks included circuits previously implicated in aspects of anxiety-like behavior in the broader literature. For example, optogenetic stimulation of the amygdala→infralimbic cortex circuit, a component of Electome Network 1, has been shown to increase anxiety-behavior during the EPM and BOF in mice [19]. Mouse studies have described increased activity in the ventral hippocampus→prefrontal cortex circuit in the EPM and BOF [12,13], and causal stimulation of this circuit increases anxiety behavior [22]. Increased coherence between amygdala and ventral hippocampus has been implicated in trait and state anxiety in human intracranial recording experiments [8] and in mediating EPM anxiety behavior in causal mouse experiments [31]. Such circuits are prominently featured in Electome Network 2. Finally, increased IL activity, as featured in Electome Network 2 and 3, drives anxiety behaviors in mice in the EPM [32]. Thus, many circuits proposed previously shown to encode aspects of anxiety were featured in our discovered electome networks.

Though our goal was to discover at least one electome network that was shared across the three anxiety paradigms, our multi-supervised network learning strategy had the potential to discover three electome networks for which each solely encoded one of the three assays. Thus, to ensure that we had indeed discovered an electome network that generalized across anxiety paradigms, we tested whether Electome Network 1, 2 or 3 encoded the anxious state in all three paradigms, again in the 20 new mice. Here we used one-tailed testing to determine whether higher activity in each network was observed in the higher context, as it had in our initial learned model. Electome Network 1 and 2 both independently generalized to all three paradigms ($P<0.05$ for all comparisons against a null distribution using a one-tailed Mann-Whitney U test) while Electome Network 3 only encoded the internal state induced by the

171 BOF assay (P = 1, P=0.66; P <0.05 for FLX, EPM, and BOF, respectively; Fig. 2D). Given that only Electome
172 Network 1 and 2 independently encoded all three assays, and Electome Network 3 only contributed 1%
173 to multi-network prediction, we limited our subsequent analysis to Electome Network 1 and 2.

174 We next probed whether the architecture of Electome Network 1 and 2 represented a brain state that
175 was shared between the three assay contexts, or whether the networks components simply represented
176 the sum of the circuits that independently encoded each of the three assays. To evaluate this question,
177 we first quantified the extent to which our two multi-assay networks could be recovered from the
178 individual assay models. Specifically, we started with the single assay-trained K-fold cross validation
179 models (from Fig. 1B), and we then selected the 3 supervised networks from the fold most predictive of
180 each assay, yielding 9 total supervised networks (3 for each assay), and performed a regression of these
181 9 networks onto Networks 1 and 2 from the multi-assay model (Fig. 2E). Finally, we evaluated the
182 quantitative fit between the multi-assay networks and the superimposed single-assay networks using
183 the cosine distance. Here a lower cosine distance indicated that a multi-assay network was similar to the
184 superimposed single-assay networks. To generate a null distribution for statistical comparisons, we used
185 three additional data sets for which there was no clear anxiety context (social interaction test, sucrose
186 countdown reward assay, and baseline recordings sleep-wake recordings). We trained 10 single-assay
187 models where the context labels (context 1 vs. context 2) were randomly assigned, generating 3 random
188 supervised networks for each of the three data sets across 10 runs. We then randomly selected 9
189 networks from these 90 learned networks (3 networks from each of the data sets) and performed the
190 same regression analysis procedure that we had initially performed using the anxiety single-assay
191 networks. This pseudorandom selection procedure was repeated 900 times, yielding a null distribution
192 consisting of 900 cosine distances between the multi-assay networks and the unrelated single-assay
193 networks that composed our regression analysis (Fig. 3E). A cosine distance less than 95% of this null
194 distribution is equivalent to P<0.05, as the expected recovery is one-tailed.

195 The cosine distance between Electome Network 1 and the composite regression of the 9 supervised
196 models (3 for each of the individual anxiety assays) was 0.14. This distance was less than 99% of the null
197 distribution (Fig. 2F, left), providing statistical evidence that Network 1 may indeed represent a
198 superposition of the single assay networks. On the other hand, the cosine distance between Electome
199 Network 2 and the composite regression of the 9 supervised models was 0.39. This distance was only
200 less than 4% of the null distribution (Fig 2F, right), providing evidence that Electome Network 2 was not
201 a superposition of the single-assay networks.

202 Since we had previously found that the single-assay networks trained for the EPM assay generalized to
203 the BOF assay, and vice versa, our initial statistical approach did not allow us to disambiguate as to
204 whether Network 1 represented a superposition of distinct individual assay networks, or whether
205 Network 1 was strongly influenced by a single network that was shared between the EPM and BOF
206 assays. Thus, to further probe this question further, we retrained a new multi-assay model in which only
207 the FLX and saline labels were reversed in the training set (FLX-reversed) while the EPM and BOF labels
208 were not reversed. Based on our prior results, we expected that: (1) we would still recover Network 1 as
209 it is primarily based on EPM and BOF; (2) this new FLX-reversed multi-assay network would classify FLX
210 as the saline context and saline as the FLX context in holdout animals, and (3) we would fail to recover
211 Network 2 since our initial analysis suggested it was dependent on all three assays.

212 All three supervised networks within the FLX-reversed multi-assay model generalized to holdout mice,
213 predicting home cage vs. EPM, home cage vs. BOF, and reversed fluoxetine vs. reversed saline
214 conditions. When we evaluated whether this procedure recovered the original Electome Network 1,
215 again using the cosine distance, we found that the supervised FLX-reversed networks showed cosine

distances of 0.71, 0.76, and 0.02 from Network 1 (Fig. 2G, left). To evaluate the significance of smallest network distance, we trained 900 anxiety-null multi-assay models for which the labels (low anxiety vs. high anxiety) for all three assays were randomly permuted. Finally, we constructed a null distribution by choosing the supervised network with the smallest cosine distance from Network 1 for each permutation. This lowest cosine distance between the three FLX-reversed multi-assay networks and Network 1 (i.e., 0.02) was lower than all the values in the null distribution (Fig. 2G, left). Thus, Network 1 was still recovered under FLX-reversed training. However, when we repeated this approach using Network 2, we found that its lowest cosine distance with one of the three networks from the FLX-reversed multi assay model was 0.48. This cosine distance was indistinguishable from the null distribution (P=0.32; Fig. 2G, right), meaning that Network 2 was not recovered under FLX-reversed training. Taken together, these results established that Network 1 represented a network that was likely shared between the EPM and BOF assays, with a small input from the FLX assay. In contrast, Electome Network 2 represented an internal state that was shared across all three assays. Thus, we focused our subsequent analysis on Electome Network 2 (heretofore referred to as *Electome Network-Anxiety*; *EN-Anxiety*).

Finally we also verified that *EN-Anxiety* generalized to female mice in the EPM assay (AUC=0.64±0.04, U=5, P= 0.0012 using a one-tailed paired Wilcoxon signed rank test; N=13 female mice), and the BOF assay using one-second windows (AUC=0.56±0.03, U=8, P= 0.048 using a one-tailed paired Wilcoxon signed rank test; N=9 female mice). As expected, encoding strength of these two assays increased with larger window sizes (see Supplemental Figure S7). Conversely, *EN-Anxiety* failed to generalize to female mice in the FLX assay (AUC=0.46±0.03, U=27, P= 0.90 using a one-tailed paired Wilcoxon signed rank test; N=8 female mice). When we explored this lack of generalization in the FLX assay, we found that treatment with fluoxetine (10mg/kg, i.p.) did not increase behavioral inhibition or heart rate in female mice (Supplemental Fig. S11). Thus, in female mice, the FLX assay failed to meet our operational definition of anxiety in female mice. Taken together, these results showed that *EN-Anxiety* selectively generalized to anxiety contexts in female mice. Notably, we also used a one-tailed statistical test for this analysis and our subsequent network validation testing, since no change in network activity or a decrease in network activity in the high anxiety setting both equally reflected a failure of our learned *EN-Anxiety* to generalize to female mice. This approach also allowed us to limit the number of mice utilized for each assay, ultimately enabling us to probe network activity across a much broader range of anxiety-related (and control) contexts (see Methods – Statistical Analysis Philosophy).

EN-Anxiety activity encodes features of anxiety-related paradigms.

We further validated *EN-Anxiety* by examining network activity dynamics during various anxiogenic events both within the training assays (i.e., FLX, EPM, and BOF) and in new experimental contexts that controlled for confounding emotional states. All analyses were performed on subjects that were not used in model training.

Within the FLX-training assay, we observed that the activity of *EN-Anxiety* decreased over time across the neural recording period in the saline- and FLX-treated mice ($F_{59,472}$=2.88, P=0.038 for time effect across minutes for *EN-Anxiety*, respectively, using a within-within two-way ANOVA with correction). As expected, given the AUC values we reported for the FLX assay in these same animals (see Fig 1E), the activity of *EN-Anxiety* was higher in the fluoxetine-treated group ($F_{1,8}$=14.81, P=0.005 for the treatment effect of the ANOVA). Nevertheless, no differences in the time effect were observed between the treatments ($F_{59,472}$=1.49, P=0.22 for treatment × time interaction effect, using two-way ANOVA with multiplicity correction; see Fig. 3A). Thus, following handling and the experimental injection, activity in

EN-Anxiety decreased the longer mice they were in their home cage. These findings provided additional evidence that *EN-Anxiety* tracked the internal anxiety state of the mice.

To further explore whether network activity decreased over time following exposure to other anxiogenic stimuli, we also analyzed network activity in the EPM and BOF, relative to the activity observed in the home cage. We focused on periods during which mice were in the closed arms of the EPM or the periphery of the BOF, since these are considered the safe zones of the assays. This approach also enabled us to control for changes in network activity that may be location specific. Activity in *EN-Anxiety* increased sharply after the mice were first placed in the behavioral areas then decreased over time across the remaining of the 5-minute testing session (Fig. 3B; T=-11.116, P<0.001 for time effect for *EN-Anxiety*, using an ANCOVA; note that task activity is depicted normalized to home cage activity). Thus, network activity in both assays paralleled the response we observed in the FLX assay. Next, we tested whether activity in the networks was behaviorally relevant. Specifically, since we found that the BOF induced higher network activity than the EPM (Fig. 3B; T=13.248, P<0.001 for assay effect using an ANCOVA of assay and time), we analyzed the behavioral profiles of mice in both assays to determine whether the BOF induced greater anxiety-related behavioral avoidance. After verifying that the mice spent substantially more time in the safe zones vs. avoidance zones in both assays (T_{10}=19.9; P<10^{-8} and T_8=29.8; P<10^{-8}, for EPM and BOF, respectively, using a one-tailed paired t-test, Fig. 3C), we quantified the bout length when animals occupied the avoidance zones. The bout length in the center zone of the BOF was significantly shorter than the bout length in the open arm for the EPM (T_{18}= 2.6; P=0.009, using a one-tailed unpaired t-test, Fig. 3C), demonstrating that the mice exposed to the BOF showed higher anxiety-related avoidance. Mice avoided the center of the BOF more during the first half of the assay, compared to the second half (T_8=3.97 and P=0.004 using a two-tailed paired t-test; see Fig. 3E). In contrast, no such behavioral pattern was observed in the EPM (Fig. 3D); mice showed large variability for when they occupied the open arms (T_{10}=0.70 and P=0.50 using a two-tailed paired t-test). These results suggested that mice were most likely to exhibit behavioral inhibition/avoidance when *EN-Anxiety* activity was highest (first half of the BOF).

To directly explore the relationship between *EN-Anxiety* and avoidance behavior, we tested whether network activity encoded occupancy of the avoidance zone on a moment-to-moment basis within the assays. Specifically, we reasoned that three distinct patterns of anxiety could intersect with behavior: 1) mice might show higher anxiety when they occupy the avoidance zones of the assay, which could be indicated by higher network activity in open arm/center vs. closed arm/surround; 2) the avoidance zone of the assays might induce a feeling of anxiety that increases over time irrespective of the animal's future location, observed as higher network activity seconds after mice are located in the open arm/center vs. seconds after they are located in the closed arm/surround; and 3) high anxiety might preclude mice from occupying the avoidance zones [31], such that higher network activity would be observed if mice occupy the closed arm/surround in the future vs. when mice occupy the open arm/center. Thus, we determined whether *EN-Anxiety* showed activity consistent with any of these 3 patterns. Importantly, though all data recorded during the EPM and BOF assays were used to discover our putative anxiety networks, the moment-by-moment location of the mice in the EPM and BOF (avoidance zone vs. safe zone) was not. Thus, this analysis tests the relationship between *EN-Anxiety* activity and behavior based on information that was not used during model training.

We first isolated all the one-second intervals when mice occupied the open or closed arm of the EPM. We also isolated neural activity up to five seconds prior to and up to five seconds following these timepoints [15,31]. *EN-Anxiety* failed to encode whether mice were in the open vs. closed arms of the EPM (U=41 and P=0.26, using a one-tailed paired Wilcoxon signed rank test; Fig. 3F); this failed to support the first pattern of anxiety-related network activity listed above. On the other hand, we found that *EN-*

306 *Anxiety* activity (U=61 and P=0.0049 using a one-tailed paired Wilcoxon signed rank test) was higher in
307 the five seconds interval following the open arm location of mice (regardless of whether they returned
308 to the closed arm during this period). Thus, an increase in *EN-Anxiety* activity was induced by the
309 avoidance zone of the assay, providing support for the second pattern listed above. No difference in
310 network activity was observed in the 5-second interval preceding the open arm location (regardless of
311 the location of the mouse during this interval), compared to activity preceding the closed arm of the
312 EPM (U=27 and P=0.32, using a one-tailed paired Wilcoxon signed rank test; Fig. 3G). This failed to
313 support the third pattern for which high network activity might preclude entrance into avoidance zones.

314 *EN-Anxiety* also failed to encode whether mice were in the center or periphery of the BOF (U=20 and
315 P=0.63 using a one-tailed paired Wilcoxon signed rank test), again showing a lack of support for the first
316 pattern. However, when mice occupied the center of the BOF, the network showed lower activity within
317 the preceding 5 seconds, compared to the five seconds preceding when mice occupied the periphery
318 (U=8 and P=0.049, one-tailed paired Wilcoxon signed rank test, Fig. 3G). Together, this finding showed
319 that high activity in *EN-Anxiety* encoded that mice would be in the safe zone of the BOF in the future,
320 thus supporting the third pattern. No increases in *EN-Anxiety* were observed in the 5-second interval
321 following the center location compared to activity when mice were in the periphery in the BOF (U=13
322 and P=0.88 using a one-tailed paired Wilcoxon signed rank test). Overall, these results showed that *EN-*
323 *Anxiety* activity was increased by the open arms of the EPM, while high activity in *EN-Anxiety* encoded
324 avoidance of the center zone in the BOF. This latter pattern of activity was consistent with our
325 observation that mice occupied the center zone less during the first half of the BOF when activity in both
326 networks was highest. Thus, *EN-Anxiety* was behaviorally relevant and supported two out of three of our
327 patterns of anxiety-related network activity, though the pattern for which aspects of anxiety behavior
328 were encoded varied between the two assays.

329 ***EN-Anxiety activity does not encode arousal or reward***

330 As arousal is a component of our operational definition of anxiety, our training approach could plausibly
331 discover networks that reflect an arousal state rather than anxiety. To explore this possibility, we
332 quantified *EN-Anxiety* activity during distinct sleep-wake arousal states. Specifically, we recorded
333 animals for 12 hours and identified intervals in which animals were in the middle of long bouts of
334 wakefulness, and when they were in rapid-eye-movement sleep (REM sleep)[33]. Though REM sleep is
335 characterized by fast brain activity, the body shows broad atonia, and animals are less responsive to
336 external stimuli. As such, it is considered a lower arousal state than wakefulness. Muscle activity was
337 higher during the awake period compared to the REM sleep intervals (U=36, P=0.0039 using a one-tailed
338 paired Wilcoxon signed rank test; N=8 mice). This was consistent with our sleep-wake classification
339 approach[33] and reflected the higher arousal state that characterizes wakefulness.

340 We reasoned that *EN-Anxiety* activity would be higher during wakefulness compared to REM if the
341 network directly encoded arousal, rather than anxiety more broadly. Though *EN-Anxiety* activity was not
342 significantly higher during wakefulness (U=24, P=0.23, one-tailed paired Wilcoxon signed rank test), such
343 a finding might reflect an inability of networks discovered using our approach to encode differences
344 between wakefulness and REM. To exclude such a possibility, we also tested another network from our
345 prior work that encodes social appetitive behavior (*EN-SocialAppetitive*, Fig. 4E, see also Supplemental
346 Fig. S12)[26]. We reasoned that this network would show higher activity during wakefulness, compared to
347 sleep. Importantly, this network is composed of the same brain regions as *EN-Anxiety*. When we
348 projected the data from the awake and REM sleep intervals into this electome network, we found that
349 activity in this network was indeed significantly higher during wakefulness vs. REM sleep period (U=32,
350 P=0.027, one-tailed paired Wilcoxon signed rank test). Thus, changes in affective network activity could

351 indeed be captured between waking and REM sleep by a network composed of the same brain regions
352 as *EN-Anxiety*. Together, these results showed that *EN-Anxiety* did not simply encode arousal.

353 We next tested whether increases in *EN-Anxiety* network activity were specific to anxiety, using data
354 acquired from two independent assays that are thought to increase reward but not anxiety. During
355 these assays, data was collected from the same brain regions used initially for model training, and LFP
356 activity was projected into the previously learned multi-assay trained model to calculate the activity of
357 *EN-Anxiety* for each second. In the first assay, nine mice were trained to maintain a nose poke for 5
358 seconds (see Supplemental Fig. S13). Tones of decreasing pitch were played throughout the 5-second
359 trial, and a 5µL sucrose reward was delivered at the end if mice remain in the port for the entire 5
360 seconds. When we tested whether reward delivery increases *EN-Anxiety* activity, we failed to identify a
361 significant increase in *EN-Anxiety* (U=41 and P=0.99, using a one-tailed paired Wilcoxon signed rank test;
362 N=9 mice, Fig. 4G). Next, we quantified *EN-Anxiety* during a classic social preference assay, where mice
363 freely explore an object and a novel social stimulus mouse housed at the two ends of a chamber. In this
364 assay, the social stimulus mouse is considered both arousing and rewarding, as experimental mice
365 generally choose to spend more time with the other mouse than the object, and social encounters
366 activate reward circuitry[34]. When projected LFP data collected in a prior study into *EN-Anxiety*[26], we
367 failed to discover increases in *EN-Anxiety* during interactions with the stimulus mouse, compared to the
368 inanimate object (U=47 and P=0.74, using a one-tailed paired Wilcoxon signed rank test, N=12 mice, Fig.
369 4H). Together, these results demonstrate that *EN-Anxiety* fails to generalize to arousal and reward, as no
370 increase in network activity is observed during higher arousal states, and network activity does not
371 increase during innate and trained-reward states.

372 ***EN-Anxiety activity encodes the internal state induced by additional anxiety paradigms***

373 We further probed whether *EN-Anxiety* encodes a robust anxiety-related brain state using additional
374 paradigms that induce anxiety in a manner that is distinct from our initial assays. Again, all analyses
375 were performed on new mice that were not used during model training. We first examined network
376 activity during direct optogenetic stimulation neurons in the ventral hippocampus. This region has been
377 causally implicated in anxiety in rodents [35], and it was a critical upstream node in *EN-Anxiety*. Moreover,
378 we selectively stimulated the subset of neurons that projected to lateral hypothalamus since the ventral
379 hippocampus→ lateral hypothalamus circuit had been shown to drive anxiety-related avoidance in the
380 EPM and BOF [20]. Mice were infected with an adenoassociated virus (AAV) to express Channelrhodopsin-
381 2 using (ChR2) in the ventral hippocampus and implanted with microwires to target the same regions
382 utilized to learn our multi-assay trained *EN-Anxiety*. A microwire and optic stimulating fiber was also
383 implanted in lateral hypothalamus, concurrently (Fig. 5A).

384 After verifying that stimulation of the ventral hippocampus → lateral hypothalamus recapitulated the
385 anxiety/avoidance behaviors described in the prior work (t_{16}=1.83, P=0.047; t_{11}=4.09, P=8.9x10^{-4} for BOF
386 center occupancy and real-time stimulation side occupancy, respectively, for comparisons of yellow and
387 blue light stimulation, one-sided t-test, reflecting the *a priori* hypothesis that circuit stimulation would
388 increase anxiety behavior; see Fig. 5B)[20], we stimulated the implanted mice with blue light to activate
389 ChR2, or yellow light as a negative control, while neural activity was recorded in their home cage. As
390 expected, blue light induced local and remote LFP activity, while yellow light did not (Fig. 5C). When we
391 projected neural activity recorded during these stimulations into our learned multi-assay trained model,
392 we found that ventral hippocampus → lateral hypothalamus stimulation increased *EN-Anxiety* activity
393 (U=0 and P<0.001, using a one-tailed paired Wilcoxon signed rank test, Fig. 5D). Stimulation of this
394 circuit failed to increase *EN-SocialAppetitive* activity in the mice (U=22 and P=0.18, using a one-tailed
395 paired Wilcoxon signed rank test, Fig. 5E), demonstrating the circuit's selectivity in driving network

activity. In control studies, we also found that stimulation of a ventral hippocampus → basal amygdala circuit (Fig. 5F), which did not induce anxiety (t_{16}=0.01, P=0.50; t_{16}=0.48, P=0.32 for BOF center occupancy and real-time stimulation side occupancy, respectively, for comparisons of yellow light and blue light stimulation using a one-tailed t-test; see Fig. 5G), failed to significantly increase *EN-Anxiety* (U=35 and P=0.08, using a one-tailed paired Wilcoxon signed rank test, Fig 5H-I). This stimulation had no impact on *EN-SocialAppetitive* as well (U=21 and P=0.46, using a one-tailed paired Wilcoxon signed rank test, Fig. 5J). Together, these data further validate *EN-Anxiety* as a specific network-level code for anxiety.

We subsequently examined whether *EN-Anxiety* encodes the internal state induced by fear conditioning. In this classic paradigm, mice are exposed to seven repeated auditory cues (conditioned stimuli, CS+), each paired to a foot shock (unconditioned stimulus, US). On a subsequent recall session, conditioned mice exposed to the auditory cue in the absence of the foot shock typically exhibit a freezing response. For our conditioning paradigm, we substituted the foot shock with a high-pressure air puff during conditioning (Fig. 5K). This enabled us to minimize electrical noise during LFP recording. Mice exposed to our modified air puff stimulus exhibited increased freezing behaviors during the recall session on a subsequent day, compared to controls (CS-) (U=439 and P=2.1×10^{-4} using a one-tailed Mann-Whitney U test; Fig. 5L). This confirmed that mice exhibited vigilance patterns that facilitated the association of a threat (US) with the context it was experienced (CS+) during the initial pairing session, meeting our operational definition of anxiety.

We then analyzed *EN-Anxiety* activity at the final stimulus of the aversive conditioning (i.e., the 7th tone), since we reasoned that the six preceding air puffs were sufficient to induce vigilance in the mice. Specifically, we compared *EN-Anxiety* activity immediately prior to and during the 7th tone between the CS+ and CS- mice. Here, we found a significant group by tone interaction effect ($F_{1,28}$=4.62; P=0.04 using a two-way repeated measures ANOVA, N=13 and 17 for CS+ and CS- mice, respectively; see Fig. 5M and 5N). Compared to the CS- control mice, *EN-Anxiety* activity was significantly elevated in CS+ mice during (t_{28}=2.37; P=0.0124 using one-tailed t-test, Fig. 5N), but not prior to the presentation of the 7th tone (t_{28}=0.82; P=0.21 using one-tailed t-test, Fig. 5N). Importantly, our post-hoc analysis found no difference in *EN-Anxiety* prior to or during the first tone exposure (i.e., preceding the first air puff in CS+ mice; $F_{1,1}$=10^{-4} and P=0.99 for group effect, $F_{1,28}$=0.55 and P=0.46 for tone effect, $F_{1,28}$=0.56 and P=0.46 for group × tone effect using a two-way repeated measures ANOVA; see Supplemental Figure S14). As such, *EN-Anxiety* encodes an acute internal state generated by the presentation of a threat-paired stimulus.

Finally, having discovered that *EN-Anxiety* encoded threat presentation during hypervigilance, but not arousal or reward, we asked whether either network broadly encoded an acute negative experience. Specifically, while anxiety is a negative affective state, not all negative experiences produce anxiety. Thus, we further probed our fear conditioning paradigm data to test whether the *EN-Anxiety* increased acutely during an ongoing negative experience. We reasoned that prior to conditioning, the first air puff should immediately invoke negative affect, but not anxiety. As such, we compared *EN-Anxiety* activity in the CS+ mice while they experienced the first air puff to network activity in CS- mice, which did not receive an air-puff. Using this approach, we found that the air puff failed to acutely increase *EN-Anxiety* activity (U=80 and P=0.53, using a one-tailed Mann-Whitney U test, Fig. 5O). These results indicated that *EN-Anxiety* activity was indeed specific for anxiety and not a generalized negative affective state.

EN-Anxiety activity is altered in mouse models of mood disorders

Anxiety can be altered in mood disorders. Indeed, bipolar mania is characterized by impulsivity and risk taking[36] (reflective of decreased anxiety processing), while major depressive disorder is highly co-morbid with high anxiety[37]. Mouse models of mood disorders have played a key role in investigating the

441 mechanisms underlying these changes in anxiety. For these models, anxiety states in mice are generally
442 inferred using assays such as the EPM. Yet, it is widely known that EPM behavior is shaped by other
443 domains of affective function that are also altered in mood disorders (i.e., psychomotor activity, see Fig.
444 6A). Thus, illness related changes across broader affective systems of mouse models can obscure the
445 relationship between EPM behavior and the true anxiety state of mice. Having robustly established and
446 validated *EN-Anxiety*, we reasoned anxiety levels could be directly assayed in mouse models of mood
447 disorders by quantifying network activity.

448 First, we tested whether a mouse model of mania shows lower *EN-Anxiety* activity in a context that
449 should otherwise induce a high anxiety state. We also tested whether two mouse models of depression
450 show high *EN-Anxiety* activity in a context that would normally be marked by a low anxiety. Namely,
451 the *ClockΔ19* mouse line has been proposed as a model of bipolar mania [38]. These mice have a point
452 mutation in the circadian gene *Clock* and exhibit altered circadian rhythms, psychomotor hyperactivity,
453 increased reward drive, and decreased avoidance in anxiety assays [15,38,39]. Moreover, many cellular,
454 neurophysiological, and behavioral alterations in these mutant mice are normalized by chronic lithium
455 or valproic acid treatment [38,40,41], providing further validation for the *ClockΔ19* mouse as a model of
456 bipolar mania.

457 We reasoned that if Clock gene disruption altered anxiety, we would observe failure of *EN-Anxiety* to
458 activate in response to EPM exposure, or an overall decrease in their *EN-Anxiety* activity. After
459 confirming that *ClockΔ19* mice demonstrate increased open arm exploration in the EPM at 20 lux
460 compared to wild-type littermate controls (t_{32}=2.90, P = 0.0033 using unpaired one-tailed t-test, Fig. 6B),
461 we implanted male and female *ClockΔ19* mice on a Balb/c background (N=18 mice) and their wild-type
462 littermate controls (N=17) with microwires targeting the same brain regions used to learn our electome
463 networks. We then quantified neural activity while mice were in the home cage and on the EPM. For
464 these experiments, we used the same light intensity we had implemented in the C57 mice to learn and
465 validate *EN-Anxiety* (i.e. 175 lux).

466 No differences in open arm exploration were observed across genotype at this higher light intensity
467 (t_{33}=0.51, P = 0.31 using unpaired one-tailed t-test, Fig. 6B, middle). Moreover, exposure to the EPM
468 increased *EN-Anxiety* activity in both genotypes, confirming that *EN-Anxiety* – discovered in C57 mice –
469 generalized to a new mouse strain background ($F_{1,35}$ = 14.21 and P=6.05×10^{-4} for assay effect using two
470 way repeated measures ANOVA for genotype × assay; Fig. 6C). Nevertheless, no significant genotype or
471 interaction effects were observed ($F_{1,35}$=0.008 and P=0.93 for genotype effect and $F_{1,35}$=0.73 and P=0.40
472 for genotype × assay effect using a two-way repeated measures ANOVA; Fig. 6C). Thus, gross *EN-Anxiety*
473 function remained intact in *ClockΔ19* mice. This was consistent with the behavior displayed by the
474 mutants, which showed strong avoidance of the open arm of the EPM (Open arm occupancy = 5.8±1.3%
475 and 5.2±2.1% in the unimplanted and implanted mice, respectively, Fig 6B, middle). Indeed, nearly half
476 (8 out of 18) of the implanted *ClockΔ19* mice occupied the open arm for less than 5 seconds.

477 Next, we wondered whether the clock mutant mice might lower network activity in the safe zone of the
478 EPM. When we quantified *EN-Anxiety* network activity while mice were in the closed arm, we indeed
479 observed lower *EN-Anxiety* network activity in the *ClockΔ19* mice compared to their littermate controls
480 (T=3.71, P<0.001 for genotype effect on *EN-Anxiety*, using an ANCOVA, Fig. 6D, left). The mutants also
481 exhibited higher EN-SocialAppetitive network activity in the closed arms (T=4.05, P<0.001 for genotype
482 effect on *EN-Anxiety*, using an ANCOVA, Fig. 6D, right), demonstrating that their decreased *EN-Anxiety*
483 activity was network specific. Since these observations raised the possibility that the implanted *ClockΔ19*
484 mice might experience decreased anxiety states in the safe zones compared to their wild type
485 littermates, yet show similar open arm exploration, we wondered whether genotype differences were

evident at the transition zone between the open and closed arms (i.e., namely the center zone of the EPM). Indeed, behavioral analysis showed that the implanted *ClockΔ19* mice exhibited greater occupancy of the center zone than their wild type littermates (t_{33}=2.14; P=0.02 using unpaired t-test; Fig. 6B, right).

Next, because our previous analysis in C57 mice found that occupancy of the open arm increased *EN-Anxiety* activity (see Fig 3F), and the center zone induced less avoidance in *ClockΔ19* mice compared to their wild type littermates, we hypothesized that *ClockΔ19* mice might also show reduced induction of *EN-Anxiety* activity following occupancy of the center zone. To probe this question, we isolated all 1 second periods where mice were in the center zone and determined network activity up to 5 seconds into the future, irrespective of the future location of the mice. This future network activity was normalized to the activity measured while mice were in the center zone, enabling us to compare the extent to which occupancy of the center zone impacted network activity across genotype. With this approach, we found that network activity was indeed lower in the mutants two seconds in the future (U=348 and P=0.0099 using unpaired one-tailed Wilcoxon rank sum test followed by false discovery rate correction, Fig. 6E, left), and tended to be lower 5 seconds into the future, though this difference did not survive correction for multiple comparisons (U =398 and P=0.046 using unpaired one-tailed Wilcoxon rank sum test followed by false discovery rate correction, Fig. 6E, left). No genotype differences were observed when we tested whether Clock disruption reduced *EN-SocialAppetitive* activity across these same time windows, demonstrating that the decreased *EN-Anxiety* activity was network specific (P>0.05 for all comparisons using unpaired one-tailed Wilcoxon rank sum test followed by false discover rate correction, Fig. 6E, right). Thus, *ClockΔ19* disruption decreased avoidance of the center zone of the EPM and suppressed the induction of *EN-Anxiety* in this otherwise high anxiety context. Overall, these results show that a mouse model of bipolar mania exhibits decreased function of *EN-Anxiety* in a high anxiety context, supporting the translational utility of this network.

Finally, we explored network activity in two mouse models of depression (Fig. 6F). Since anxiety is observed in major depressive disorder in contexts where anxiety should otherwise be low/absent, we hypothesized that higher *EN-Anxiety* activity would be observed when the two mouse models of depression were in the low anxiety context of their home cage. In the chronic social defeat stress paradigm, mice are repeatedly exposed to larger-aggressive mice. After 10 exposures, a subset of *susceptible* mice exhibits social avoidance, disrupted reward behavior, and anxiety-like behavior [42,43]. Conversely, the other subset of *resilient* mice exhibits normal social and reward behavior [42,43] (Fig. 6F-G). Interestingly, despite the well-described differences in appetitive behavior, prior work has reported increased open arm avoidance in the EPM in both the susceptible and resilient mice [42,44]. Indeed, exposure to chronic social defeat stress increases open arm avoidance in the EPM for both unimplanted susceptible and resilient mice uniformly (t_{20}=2.27 and P=0.02, for comparison between stress and unstressed mice using a one-tailed Welch's t-test; t_{10}=0.16 and P=0.87 for post-hoc comparison between susceptible and resilient mice using a two-tailed t-test; see Fig. 6H). Therefore, we tested whether this stress paradigm also increased *EN-Anxiety* in both the susceptible and resilient groups compared to non-stressed controls. Again, since we hypothesized that stress exposure induces anxiety – and therefore higher *EN-Anxiety* activity – in contexts where anxiety is not observed under normal conditions, we quantified network activity from stress and unstressed mice while they were in their home cage. Here, we found significantly higher *EN-Anxiety* activity in the stressed mice (U=151 and P<0.01 using one-tailed Mann-Whitney U test, Fig. 6I, left). Moreover, no difference in *EN-Anxiety* activity was observed between susceptible and resilient mice (U=382 and P=0.62, for post-hoc analysis using a two-tailed Mann-Whitney U test, Fig. 6I, right). Finally, no increases in *EN-SocialAppetitive* activity were observed demonstrating that the stressed induced changes in *EN-Anxiety* activity were network specific (U=397, P= 0.41 using one-tailed Wilcoxon Rank sum test, Fig. 6J). Thus, chronic social defeat stress increased *EN-Anxiety*

activity in both susceptible and resilient groups of mice (which both exhibit anxiety). Importantly, this stress-induced increase in *EN-Anxiety* was observed in the home cage context, which otherwise facilitates a low anxiety state.

We next quantified network activity in mice exposed to chronic mild unpredictable stress. In this paradigm, mice are repeatedly exposed to a series of stressors over eight weeks. Specifically, test mice are subjected to two stressors per day, one occurring during the light phase of their circadian rhythm cycle and the other during the dark phase. Stressors, including environmental stressors, food/water restriction, or physical restraint, were chosen according to a pseudo-randomized schedule. Exposure to this protocol induces altered reward and social behavior, as well as increased anxiety-related behavior in mice compared to their non-stress controls [45,46]. After verifying that chronic mild unpredictable stress induced open arm avoidance in the EPM (i.e., increased anxiety-related behavior; t_{19}=2.37 and P=0.018, for comparison between stress and unstressed mice using a one-tailed Welch's t-test; see Fig. 6K), we quantified *EN-Anxiety* activity in stressed mice and non-stressed controls. We again hypothesized that stress exposure induces anxiety – and therefore higher *EN-Anxiety* activity – in contexts where anxiety is not observed under normal condition. Thus, we quantified network activity from stress and unstressed mice while they were in their home cage. Like chronic social defeat stress, exposure to chronic mild unpredictable stress increased *EN-Anxiety* activity (U=81 and P=0.036, using a one-tailed Mann-Whitney U test, Fig. 6L). No such increases were observed in EN-SocialAppetitive in the stress group, demonstrating that the stressed induced change in *EN-Anxiety* activity was specific (U=101, P= 0.60 using one-tailed Wilcoxon Rank sum test, Fig. 6M). Together, these findings establish that two of the most widely utilized paradigms for modeling depression in mice converged on a common network-level signature that can be observed when mice are otherwise in a low anxiety context. Thus, these results highlight the translational utility of *EN-Anxiety* for phenotyping mouse models of mood disorders.

Discussion

Preclinical models have played a role in the development of therapeutics for emotional disorders. These efforts would be greatly enhanced by the discovery of biological mechanisms that instantiate affective internal states in health and disease. Any such mechanisms must generalize across individual animals and affective contexts to achieve their true translational potential. Here, we employed multisite electrical recordings in freely behaving mice subjected to a collection of behavioral and experimental paradigms to discover and validate an electome network that encoded such a generalized anxious internal state. We reasoned that a putative anxious internal state could be observed at the intersection of many distinct paradigms used to model and induce anxiety in mice. Moreover, we believed that the unique features of these paradigms would enable us to disambiguate this anxious internal state from other internal states, such as arousal and reward state, or other task-relevant variables (e.g., bright light, avoidance, etc., see Fig. 7A). Machine learning models trained solely using data from one anxiety paradigm failed to generalize to all three anxiogenic paradigms. On the other hand, a model trained using data from all three assays discovered a network reflecting a shared internal anxious state. Specifically, *EN-Anxiety* generalized to additional anxiety paradigms, including direct optogenetic interrogation of a circuit originating from a key network node (VHip) and a classic fear conditioning assay, highlighting its sensitivity. Finally, *EN-Anxiety* failed to encode multiple behavioral assays that induce rewarding and/or arousing (but not anxious) internal states, demonstrating its specificity (Fig. 7B). Thus, our multi-assay learning approach discovered a generalized anxious brain state.

While each of our initial three paradigms could be encoded by LFP activity from at least one implanted region, no single brain region could independently encode an internal state shared across the three

578 paradigms. Previous findings have established that a circuit involving amygdala and ventral
579 hippocampus encodes anxiety in the EPM task in mice[31]. Indeed, we were also able to decode anxiety in
580 the EPM and BOF solely using LFPs recorded from these two areas (power across both regions, and the
581 coherence and Granger directionality measures between them). Yet, we were unable to capture an
582 anxiety state shared across all three assays solely using LFP activity from amygdala and ventral
583 hippocampus, or any other pairs of brain regions we recorded in this study. This suggests that activity
584 within a given brain region or circuit can capture some behavioral/affective features of an individual
585 assay, while failing to independently encode a generalized anxiety state shared across all three assays.
586 For example, activity in a region/circuit may encode non-specific neural responses to the induction
587 paradigms (e.g., sensing a bright light, or non-specific drug effects like large scale serotonin increases in
588 the brain), or behavioral features that correspond with anxiety in at least one of the three assays (e.g.,
589 locomotion). Because we employed different anxiety induction protocols (bright light, elevated arena,
590 drug injection) and behavioral contexts (novel testing arena vs. home cage), we encouraged our machine
591 learning strategy to discover a network-level, generalized anxiety state rather than circuits that encode
592 specific features of each assay. Therefore, we assert that while many individual regions or circuits may
593 contain assay-relevant information, the anxious brain state is optimally represented at the network-level,
594 where activity across many distinct brain regions/circuits is integrated at the sub-seconds timescale.
595 Taken together, our findings highlight two important principles to help discover the neural architecture
596 underlying affective states: 1) employ multiple distinct paradigms to discover generalized affective states
597 rather than simply encoding features of an assay, and 2) use neural activity acquired from multiple brain
598 regions [24].

599 We do not contend that the learned *EN-Anxiety* provides a comprehensive description of the anxious
600 internal state. Rather, we believe that this network-level state is also coupled with physiological changes
601 across brain regions involved in sensory and motor function, and throughout the body. It is also likely
602 that several neural circuits outside of *EN-Anxiety* can converge to impact its activity. Indeed, we found
603 that stimulating ventral hippocampal projections in lateral hypothalamus – a region that is not utilized to
604 learn *EN-Anxiety*– increased *EN-Anxiety* activity. Thus, we assert *EN-Anxiety* provides a robust and
605 objective neural measure of the internal state that mediates anxious behavior.

606 In addition to robustly encoding anxiety contexts, we also discovered that the *EN-Anxiety* encoded
607 location dependent aspects of commonly utilized anxiety assays. Specifically, *EN-Anxiety* encoded
608 occupancy of the avoidance zone in the EPM and BOF. In the BOF, high network activity encoded
609 avoidance of the center zone in the immediate future (Fig. 3G), while in the EPM, high network activity
610 encoded occupancy of the open arms in the immediate past (Fig. 3F). Thus, although these tasks are
611 widely considered to be interchangeable assays for quantifying anxiety states in mice, we found that the
612 pattern of *EN-Anxiety* encoding was distinct between the assays. Our behavioral analysis provided
613 further support for the existence of key anxiety-related distinctions between the two tasks. Mice
614 occupied the EPM avoidance zone throughout the assay (Fig. 3D), while mice showed greater occupancy
615 of the BOF avoidance zone in the second half of assay vs. the first half (Fig. 3E). This observation was
616 consistent with the high *EN-Anxiety* activity we observed during the first half of the BOF (Fig. 3B). Finally,
617 we found no relationship between avoidance in the EPM and avoidance in the BOF when we recorded
618 mice in both assays (Supplemental Fig. S2, bottom). Thus, while both assays engage key anxiety circuitry,
619 we pattern whereby anxiety circuits shape behavior may be distinct across these two assays.

620 Supporting the translational utility of our *EN-Anxiety*, we quantified network activity in a mouse model
621 of mania and two well-established preclinical animal models of depression based on chronic stress
622 exposure. The mouse model of mania exhibits predictive validity as it shows increased reward drive and
623 decreased anxiety-like behavior that responds to chronic lithium treatment [38]. Mutant mice exhibited

normal gross *EN-Anxiety* network function (i.e., *EN-Anxiety* encoded the difference between low vs. high anxiety context in the mutants). Yet, we also found that the network's encoding in relationship to EPM avoidance zones was blunted in the mutants. Thus, in addition to our prior work which established that the mutant's deficits in anxiety behavior may be shaped by altered activity in reward circuits[15], these findings argue that deficits in precise *EN-Anxiety* coding may play a role as well.

Both stress models we tested exhibit predictive validity with depression as they produce heightened anxiety-like behavior and an anhedonia phenotype that responds to chronic antidepressant administration [43,47,48]. We observed increased *EN-Anxiety* activity in both depression models when mice were in a context that is otherwise characterized by low anxiety (i.e., in their home cage), further arguing for their face validity as a model of stress pathology. Taken together, our findings establish a brain electome network that encodes anxiety-behavior in otherwise healthy animals and altered anxiety states in mouse models of mood disorders. Thus, we contend that *EN-Anxiety* presents a putative preclinical biomarker for phenotyping mouse models and for the development of anxiolytic therapeutics.

Figure Legends

Figure 1: Distributed electome networks encode anxiety states across multiple anxiety-related paradigms. A) Local field potential oscillations recorded concurrently from 8 brain regions (left), as mice were subjected to three distinct paradigms used to induce low (LA) and high anxiety (HA) states respectively (middle column): acute injections of saline vs. fluoxetine (top), home cage vs. elevated plus maze (middle row), and home cage vs. bright open field (bottom). Heart rate measures for each assay are shown to the right, and comparisons between the LA and HA states were performed using a one-tailed t-test ($P<0.05$ for all comparisons, N=7-9 male mice per assay). **B)** dCSFA-NMF results when the network model was used to discover an electome network for each anxiety paradigm. Electome networks learned for the three anxiety paradigms were applied to new mice subjected to the three paradigms (N= 13, 26, and 19 training mice for FLX, EPM and BOF, respectively, and N= 6, 11, 9 holdout testing mice for FLX, EPM and BOF, respectively). Nine generalization tests for each of the three learned networks were run in new mice subjected to the three different anxiety paradigms. C) Schematic of electome-based decoding of anxiety from multi-region LFP activity. Multi-region LFP recordings are segmented into discrete time windows and converted into feature vectors describing oscillatory power, coherence, and Granger causality. These features are decomposed into a set of electome networks, producing window-specific network activity scores. A supervised model maps a subset of the network activities to an anxiety state for each window, while the learned network weights allow reconstruction of LFP features from network activity, providing interpretability of the latent network representations. **D)** Network Consistency was evaluated by training the dCSFA-NMF model multiple times, where the mice used for training and validation were shuffled. A cosine distance metric quantified the consistency of the supervised networks across runs, where a lower cosine distance reflected greater network consistency. **E)** Box and whisker plots show generalization tests, for which the networks learned from the multi-assay dCSFA-NMF model were applied to new mice (same mice as Fig. 1B) subjected to the three different anxiety paradigms. Horizontal dashed line at AUC = 0.5 corresponds to models with no predictive utility. For the box and whisker plots, the central mark is the median, the edges of the box are the 25th and 75th percentiles, the whiskers extend to the most extreme datapoints the algorithm does not consider to be outliers. **F)** Predictive utility of multi-region multi-assay dCSFA-NMF network model (same as Fig. 1E) vs. models solely based on activity from single brain regions. Models that showed significant encoding are highlighted in pink (data analyzed using a single-sample t-test against a null AUC

distribution at α = 0.05 and shown as mean±s.e.m). Note that only the network model encoded all three assays.

Figure 2: Individual electome networks within the multi-assay anxiety model independently encode distinct anxiety paradigms. A) Power, coherence, and Granger directionality measures that comprise each electome network. Brain regions and frequency bands ranging from 1–56 Hz are shown around the rim of the plot. Power features are depicted as bands within the rim of the plot, and cross-spectral coherence measures are depicted by the lines connecting the brain regions through the center of the circle. The top 15 percent of components for each electome network are shown. **B)** Granger causality was used to quantify directionality for the coherence measures shown in A. Prominent directionality features were found in multiple bands coded by color. Histograms quantify the number of lead and lagging circuit interactions for each brain region. **C)** Schematic of directionality for each of the three electome networks. Arrows are colored to represent the dominant frequency of directionally (see color scale in panels A or B). **D)** Independent predictive performance of each supervised network across each anxiety assay. Mean contribution towards the joint model logistic regression predictions is also shown as the weight listed above each network's graph. Tests were performed using the 17 holdout mice, and networks that showed significant encoding are highlighted in pink (data analyzed using a one-tailed unpaired t-test against a null AUC distribution at α = 0.05. Horizontal dashed line at AUC = 0.5 corresponds to models with no predictive utility. Data shown as mean±s.e.m.). **E)** Coefficient weights for networks learned using individual assays (Fig. 1B and Supplemental Fig. S3) regressed onto Network 1 (left) or Network 2 (right). Cosine distances quantifying the difference between the individual assay regression network and the multi-assay network networks are shown. **F)** Distribution of cosine distances between Network 1 (left) or Network 2 (right) and 900 regression networks generated from three assays of affective states orthogonal to anxiety. Each null distribution was compared to the cosine distances described in E. **G)** Distribution of cosine distances between Network 1 (left) or Network 2 (right) and 900 multi-assay networks generated by randomly permuting the anxiety labels (low anxiety vs. high anxiety). The colored vertical lines indicate the cosine distances for the three networks learned using a model in which the fluoxetine and saline labels were reversed. The smallest cosine distance is highlighted in red. Network 2 is heretofore referred to as *EN-Anxiety*.

Figure 3: *EN-Anxiety* activity encodes features of anxiety related paradigms. A) *EN-Anxiety* activity dynamics during fluoxetine assay. Data is plotted across 5-minute windows for *EN-Anxiety*. Note that activity decreases in the network over time following saline and fluoxetine treatment (N = 9 mice). P<0.05 for time effect using a within-effects two-way ANOVA. **B)** Comparison of *EN-Anxiety* activity in safe zones of the EPM (closed arm) and BOF (periphery) over the duration of the assays. Time (P^*), and assay ($P^\#$) effects were determined using an ANCOVA (see methods). Data was plotted with a 10s sliding window and shown normalized to network activity observed in the home cage. **C)** Mice showed avoidance of the 'anxiogenic' zones of the EPM (left, P<0.01 using one-tailed paired t-test) and BOF (middle, P<0.01 using one-tailed paired t-test). Bout length of mice in the avoidance zones for EPM and BOF (right; P<0.05 using one-tailed unpaired t-test). **D-E)** Average test interval per location/mouse in safe and (see methods) anxiogenic zones in D) EPM and E) BOF assays. The vertical dashed line at 150s divides the first and second halves of each assay. Note that mice showed greater occupancy of the center in the second half of the BOF, compared to the first half. **F)** *EN-Anxiety* activity dynamics relative to arm locations in the EPM assay. Gray highlights 1 second windows when the animals are in the open or closed arms. Neural activity preceding and following these timepoints is shown as well, and data is shown normalized to the mean activity observed across the assay. The purple line highlights temporal intervals with significantly different *EN-Anxiety* activity, determined using a one-tailed Wilcoxon signed

713 rank test (N = 11 mice). **G)** Same as F, except data shown for the BOF assay (N=9 mice). Data plotted at
714 mean±s.e.m.

715 **Figure 4: *EN-Anxiety* does not encode orthogonal affective states. A)** Depiction of clustering approach
716 utilized to classify sleep-wake states (see Methods for details, unlabeled windows are shown in black).
717 **B)** Selection criteria for waking and REM sleep periods for analysis. Waking intervals were defined by at
718 least 30 seconds of waking labeled data with at least 5 minutes of >95% wake labels on both sides of the
719 data segment (top). REM sleep intervals were defined by at least 60 consecutive seconds that were
720 labeled as REM sleep (bottom). **C)** Average electromyographic activity during selected waking and REM
721 sleep intervals. **D)** *EN-Anxiety* network activity during waking vs. REM sleep periods (P>0.05 using one-
722 tailed paired Wilcoxon signed rank test). **E)** Network previously discovered to encode a social appetitive
723 brain state[26]. Brain regions and frequency bands ranging from 1–56 Hz are shown around the rim of the
724 plot. Power features are depicted as bands within the rim of the plot, and cross-spectral coherence
725 measures are depicted by the lines connecting the brain regions through the center of the circle. The top
726 15 percent of components for each electome network is shown. **F)** EN-SocialAppetitive network activity
727 during waking vs. REM sleep periods (P<0.05 using one-tailed paired Wilcoxon signed rank test). **G)** Mice
728 were trained to maintain a nose poke for 5 consecutive seconds. A sucrose reward was delivered at time
729 zero, highlighted by gray. *EN-Anxiety* activity was compared prior to and following sucrose delivery using
730 a one-tailed paired Wilcoxon signed rank test (N=9 mice). Data is shown as mean±s.e.m. **H)** *EN-Anxiety*
731 activity was quantified while mice engaged with an object or a social stimulus mouse during a free
732 interaction assay and compared using a one-tailed sign-rank test (N=12 mice). All analyses were
733 performed in mice that were not used to learn the multi-assay anxiety model. Data is shown as
734 mean±s.e.m.

735 **Figure 5: *EN-Anxiety* activity encodes distinct anxiety paradigms. A)** Mice were infected with ChR2 in
736 ventral hippocampus (VHip) and a stimulating fiber was implanted in lateral hypothalamus (LH). **B)** Mice
737 were stimulated with blue (473nm, 20Hz, 5mW, 5ms pulses) or yellow light (593.5nm, 20Hz, 5mW, 5ms
738 pulses) during testing in the BOF (left), or one side of a real-time place preference assay (N=13).
739 Comparisons of yellow light and blue light stimulation were run with a one-tailed t-test. **C)** Mice were
740 infected with ChR2 in VHip and an optrode was implanted in LH. Multiwire electrodes were also
741 implanted to target the 8 brain regions utilized to learn the multi-assay anxiety network (N=11 mice).
742 Neural activity recorded during optogenetic stimulation of VHip terminals in LH with yellow (left) or blue
743 light (right). Note that blue light stimulation of VHip induced activity in LH (and remotely) while yellow
744 light stimulation did not. **D)** *EN-Anxiety* showed an increase in activity with blue vs. yellow light
745 stimulation (P<0.001 using a one-tailed Wilcoxon signed rank test). **E)** In contrast, blue light stimulation
746 failed to increase EN-SocialAppetitive activity (P=0.18 using a one-tailed Wilcoxon signed rank test). **F)**
747 Mice were infected with ChR2 in ventral hippocampus (VHip) and a stimulating fiber was implanted in
748 amygdala (Amy). **G)** Mice were stimulated with blue or yellow light during testing in the BOF (left), or
749 one side of a real time place preference assay (N=18). **H)** Mice were infected with ChR2 in VHip and an
750 optrode in Amy. Multiwire electrodes were also implanted to target the 8 brain regions utilized to learn
751 the multi-assay anxiety network (N=11 mice). Neural activity recorded during optogenetic stimulation of
752 VHip terminals in Amy with yellow (left) or blue light (right). **I)** Blue light stimulation had no impact on
753 *EN-Anxiety* or **J)** EN-SocialAppetitive activity. **K)** Behavioral paradigm utilized to induce fear conditioning.
754 Conditioned mice (CS+; N=17) received an air puff at the end of each tone presentation, while non-
755 conditioned mice (CS-; N=20) did not (top). Neural activity was recorded in both groups throughout tone
756 presentation (bottom). **L)** Freezing behavior in CS- and CS+ mice one to two days after exposure to the
757 conditioning paradigm. **M)** *EN-Anxiety* activity relative to the 7th tone, tone onset denoted by the
758 vertical black line (N=13 CS+ and 17 CS- mice; data shown as mean±s.e.m.). **N)** Mean Activity of *EN-*
759 *Anxiety* within the interval prior ('pre-tone (10s)') or during ('tone (20s)') the presentation of the 7th

conditioning tone. Presentation of the 7th tone increased network activity in the CS+ mice (data was analyzed using a two-way repeated measures ANOVA, followed by a one-tailed t-test). **O)** Mean activity of *EN-Anxiety* in response to the first air puff (stimulus presentation shown by dark grey vertical bar; N=7 CS+ and 15 CS- mice; data shown as mean±s.e.m.). Data was analyzed using a one-tailed Mann-Whitney rank sum test. Mean network activity for the two groups is shown in the inset. For the box and whisker plots, the central mark is the median, the edges of the box are the 25th and 75th percentiles, the whiskers extend to the most extreme datapoints the algorithm does not consider to be outliers.

Figure 6: *EN-Anxiety* based assessment of anxiety function in mouse models of mood disorders. A) Schematic of how orthogonal affective states shape behavior in the EPM. **B)** EPM open arm exploration in unimplanted WT and *ClockΔ19* mice tested at 20 lux (N=17 mice/genotype, left), and implanted WT and *ClockΔ19* mice tested at 175 lux (N=17-18 mice/genotype, middle). Center occupancy time for the implanted mice is shown to the right. Data was compared using an unpaired one-tailed t-test. **C)** *EN-Anxiety* network activity while WT and *ClockΔ19* mice were in their home cage and in the EPM. Data was analyzed using a two-way repeated measures ANOVA. **D)** *EN-Anxiety* (left) and EN-SocialAppetitive (right) activity while WT and *ClockΔ19* mice were in the closed arm of the EPM. Genotype effects were determined using an ANCOVA (P<0.05 for both networks). Data shown as mean±s.e.m.**E)** *EN-Anxiety* (left) and EN-SocialAppetitive (right) activity in response to occupancy of the center zone of the EPM. Data was compared across genotype using an unpaired one-tailed rank sum test, followed by an FDR correction for each offset. **F)** Distinct stress paradigms utilized to model depression in mice. Red and green divisions in the chronic social defeat stress paradigm represent the susceptible and resilient mice that result from the paradigm, respectively (left). Pink in the chronic mild unpredictable stress paradigm represents the stressed mice subjected to the paradigm (right). **G)** Schematic of choice interaction assay utilized to quantify susceptibility to chronic social defeat stress (left), and resultant social interaction profiles of a population of stressed mice (right). Red circles denote susceptible mice (interaction ratio < 1), while green circles denote resilient mice (interaction ratio >= 1). Black circles denote non-stressed control mice. **H)** EPM open arm exploration in mice subjected to chronic social defeat stress (N=12 mice) and control mice (N=10 mice). Data was compared between stressed and non-stressed mice using a one-tailed t-test. Post-hoc testing between susceptible (N=5 mice) and resilient mice (N=7 mice) was performed using a two-tailed t-test. **I)** *EN-Anxiety* activity was quantified in the home cage and compared between chronic social defeat stressed (N=34 mice) and non-stressed controls (N=16 mice) a one-tailed Mann-Whitney rank-sum test. Post-hoc testing was compared between susceptible (N=21 mice) and resilient mice (N=13 mice) using a two-tailed Mann-Whitney rank-sum test. **J)** Comparison of EN-SocialAppetitive activity in the mice shown in G. Data was analyzed using a one-tailed rank-sum test. **K)** EPM open arm exploration in mice subjected to chronic mild unpredictable stress (N=11 mice) and control mice (N-11 mice). Data was compared using a one-tailed Welch's t-test. **L)** *EN-Anxiety* activity was quantified in the home cage and compared across groups using a one-tailed Mann-Whitney rank-sum test. **M)** Comparison of EN-SocialAppetitive activity in the mice shown in J. For the box and whisker plots, the central mark is the median, the edges of the box are the 25th and 75th percentiles, the whiskers extend to the most extreme datapoints the algorithm does not consider to be outliers.

Figure 7: Conceptual framework utilized to discover and validate an electome network for anxious internal state. A) Affective/neurophysiological states and task variables are listed on the left of the table, and they are induced by behavioral and experimental manipulations (listed along the top). Manipulations that were hypothesized to be related to the state/task variables are colored in green, while those hypothesized to decrease a state/task variable are colored in red. Manipulations for which there is no clear prediction for the impact on the state are uncolored. Responses of *EN-Anxiety* to experimental conditions utilized throughout the study are shown below. Green and red boxes highlight conditions where network activity significantly increased or decreased, respectively. Numbers of mice

807 used for each analysis are shown in the bottom row. New independent mice are highlighted in green.
808 Responses of *EN-Anxiety* to experimental conditions utilized throughout the study. Green and red boxes
809 highlight conditions where network activity significantly increased or decreased, respectively.

810

811 **Methods**

812 **Animal Care & Use**

813 Male C57BL/6J (C57) mice were purchased from Jackson Labs at 6-8 weeks of age. Unless otherwise
814 specified, mice were housed 3-5 per cage, on a 12-hour light/dark cycle, and maintained in a humidity-
815 and temperature-controlled room with water available *ad libitum. Clock*Δ19 mice were created by N-
816 ethyl-N-nitrosourea mutagenesis that produced a dominant-negative CLOCK protein as previously
817 described [39,40]. After backcrossing >10 generations on a BALB/cJ background, *Clock*Δ19 mice and their
818 wild type littermate controls were bred from heterozygous (*Clock*Δ19 -/+) breeding pairs. Male and
819 female mice, 8-16 weeks old, were used for electrophysiological experiments presented in this study.
820 Most anxiety-related manipulations and behavioral tests were conducted with approved protocols from
821 the Duke University Institution Animal Care and Use Committee, with the following two exceptions. The
822 elevated plus maze (EPM) behavioral experiments in unimplanted *ClockΔ19* mice and their littermate
823 controls were conducted at the University of Pittsburgh in compliance with approved protocols from the
824 University of Pittsburgh's Institution Animal Care and Use Committee. The EPM behavioral experiments
825 in mice exposed to chronic social defeat stress were conducted at the University of Iowa in compliance
826 with approved protocols from the University of Iowa's Institution Animal Care and Use Committee. All
827 experiments were conducted in 6-20 weeks old mice, and in accordance with the NIH guidelines for the
828 Care and Use of Laboratory Animals.

829 **Data Extraction and Processing**

830 **Electrode Implantation Surgery**

831 The electrode implantation surgery procedure has been described previously[49,50]. Mice were
832 anesthetized with 1.5% isoflurane, placed in a stereotaxic device and metal ground screws were secured
833 above anterior cranium (midline) and cerebellum (midline). A third screw was secured laterally, roughly
834 half-way between the two other screws. Thirty-two tungsten microwires were arranged in array bundles
835 designed to target amygdala (Amy, 6 microwires), medial dorsal nucleus of thalamus (MD, 3 microwires),
836 nucleus accumbens core and shell (NAc, 8 microwires), ventral tegmental area (VTA, 4 microwires),
837 medial prefrontal cortex (mPFC, 8 microwires: 4 for cingulate cortex, 2 for prelimbic cortex, and 2 for
838 infralimbic cortex), and ventral hippocampus (VHip, 3 microwires). They were centered based on
839 stereotaxic coordinates measured from bregma (Amy: -1.4mm AP, 2.9 mm ML, -3.85 mm DV from dura;
840 MD: -1.58mm AP, 0.3 mm ML, -2.88 mm DV from dura; VTA: -3.5mm AP, ±0.25 mm ML, -4.25 mm DV
841 from dura; VHip: -3.3mm AP, 3.0mm ML, -3.75mm DV from dura; mPFC: 1.62mm AP, ±0.25mm ML,
842 2.25mm DV from dura; NAc: 1.3mm AP, 2.25mm ML, -4.1 mm DV from dura, implanted at an angle of
843 22.1°). The wires targeting prelimbic cortex were built with a 0.25mm stagger anterior, and a 0.5mm
844 stagger ventral, to the infralimbic cortex wires. Wires targeting cingulate cortex were built with a 0.6mm
845 stagger anterior to the wires targeting prelimbic cortex and a 1.1mm stagger anterior to the wires
846 targeting infralimbic cortex. Animals were implanted bilaterally in mPFC and VTA. All other bundles were
847 implanted in the left hemisphere (Supplemental Fig. S15. The NAc bundle included a 0.6mm DV stagger
848 such that wires were distributed across NAc core and shell. We targeted basolateral amygdala (BLA) and
849 central amygdala) (CeA) by building a 0.5mm ML stagger and 0.3mm DV stagger into our Amy electrode

850 bundle [26]. Notably, these implantation sites have been homogenized across experimental preparations in
851 the lab enabling comparative analysis across prior and recently collected data sets. A metal ground wire
852 was secured to the anterior and posterior screws, and the implanted electrodes were anchored to all
853 three screws using dental acrylic. To mitigate pain and inflammation related to the procedure, all animals
854 except those subjected to fear conditioning, chronic mild unpredictable stress, and chronic social defeat
855 stress received carprofen (5mg/kg, s.c.). Injections were given once prior to surgery and then every 24
856 hours for three days following electrode implantation.

857 **Neural Electrophysiological Data Acquisition & Video Recording**

858 Neurophysiological data were acquired using a Cerebus acquisition system (Blackrock Microsystems, Inc.,
859 Salt Lake City, UT). Animals were connected to the system using an M or Mu-32 channel headstage
860 (Blackrock Microsystems, Inc., Salt Lake City, UT) and a motorized HDMI commutator (Doric Lenses,
861 Quebec, Canada). Local field potentials (LFPs) were bandpass filtered at 0.5–250Hz and sampled/stored
862 at 1kHz. All neurophysiological data were referenced to a ground wire connecting the ground screws
863 above cerebellum and anterior cranium. Video recordings were acquired in real-time using NeuroMotive
864 (Blackrock Microsystems, Inc., Salt Lake City, UT) and synchronized with neurophysiological data.

865 **Histological Confirmation**

866 Histological analysis of implantation sites was performed using one of two protocols at the conclusion of
867 experiments to confirm electrode placement. Animals were perfused with 4% paraformaldehyde (PFA,
868 Electron Microscopy Sciences), and brains were harvested and stored for 24 hours in PFA. Brains were
869 either processed on a cryostat or vibratome. 1) For cryostat: Brains were then cryoprotected with
870 sucrose and frozen in OCT compound prior to being stored in -80°C. Brains were sliced at 35 µm using a
871 cryostat and stained with either DAPI (AbCam) or cresyl violet (Sigma) using standard protocols. Slices
872 were imaged at 4x and 10x magnification on a Nikon eclipse fluorescent microscope. 2) Alternatively for
873 brains processed via vibratome, mice were perfused with 4% paraformaldehyde (PFA, Electron
874 Microscopy Sciences) in PBS, and brains were harvested and post-fixed in 4% PFA and then transferred to
875 PBS with 0.05mM sodium azide. Brains were sliced at 40 µm (Leica Vibrating Blade Microtome) and
876 stained with Hoechst (Fishersci) containing mounting solution (9.6% Mowiol 4-88 (Sigma) in 24%
877 glycerol, 0.M M Tris-Cl pH 8.5) on standard microscope slides. Slides were imaged at 4x and 10x with
878 Olympus Slide Scanner (VS200).

879 **LFP Processing to Remove Signal Artifact**

880 We employed a heuristic approach to eliminate recording segments containing non-physiological signals
881 identically to previous works [26,51], and we paraphrase the processing procedure as follows: we first
882 computed the signal envelope for each channel by utilizing the magnitude of the Hilbert transform. For
883 any 1-second window in which the envelope surpasses a predetermined low threshold, we discard the
884 entire segment if, at any point within that window, the envelope exceeds a second, higher threshold. The
885 two thresholds were independently determined for each brain region. The high threshold was set at 5
886 times the median absolute deviation of the envelope value specific to that region. The choice of five
887 median absolute deviations as the high threshold was based on its approximate equivalence to 3
888 standard deviations from the mean in normally distributed data, while remaining robust to outliers. The
889 low threshold was empirically established as 3.33% of the high threshold. If more than half of the
890 window was removed for a given channel, we also removed the remaining portion of that window for
891 that channel. Additionally, any windows where the standard deviation of the channel is less than 0.01
892 were excluded.

893 **Feature Extraction**

Feature extraction was performed identically to previous works [26,51], and we paraphrase the generation procedure as follows: LFPs were averaged across wires within the same region to generate a composite LFP measure. Signal processing was conducted using MATLAB (The MathWorks, Inc., Natick, MA). For LFP Power, a sliding Fourier transform with a Hamming window was applied to the averaged LFP signal utilizing a 1-second window and a 1-second step. Frequencies ranging from 1–56Hz were analyzed. LFP cross-regional coherence was computed from pairs of averaged LFPs using magnitude-squared coherence, where coherence is a function of the power spectral densities of brain regions A and B and their cross-spectral densities.

$$C_{AB}(f) = \frac{|Psd_{AB}(f)|^2}{Psd_{AA}(f)Psd_{BB}(f)}$$

Spectral Granger causality features [52] were computed using the multivariate Granger causality (MVGC) MATLAB toolbox [53]. The data underwent a high-pass Butterworth filter with a stopband at 1Hz and a passband at 4Hz. Granger directionality values for each window were calculated using a 20-order AR model through the GCCA_tsdata_to_smvgc function of the MVGC toolbox. Granger directionality values were determined for all integer frequency values within the specified range for all directed pairs of brain regions in the dataset[51].

Acute Fluoxetine Administration (FLX)

For the behavioral fluoxetine experiments, mice were randomly assigned to receiving an injection of either fluoxetine or saline 30 minutes prior to being placed on the elevated plus maze (EPM). Fluoxetine (Sigma) was made up in 0.9% NaCl to a concentration of 1mg/mL and then injected at 10mL/kg for a final concentration of 10 mg/kg, i.p.[28]. Physiologic saline injection was injected at 10 mL/kg as well as a control for injection volume. Animals were habituated to i.p. injections daily for 1 week prior to behavioral testing.

For electrophysiological recordings, animals used for training the final multi-assay model followed a standard pharmacological crossover design. Though fluoxetine only has an 8-hr half-life in mice, a lengthy washout period of two weeks was used to ensure no traces of the drug remained. Specifically, after habituation to the experimental room for 1 hour, mice were pseudorandomly assigned to receiving a fluoxetine or saline injection. Neural recordings were then obtained for an hour. Two weeks later, animals underwent a second one-hour recording session after receiving the other treatment. To test the final model, we utilized a protocol in which two recordings were performed at a much closer interval. Specifically, after habituation to the experimental room for 1 hour, nine new mice were treated with saline and neural data was recorded for an hour. Several hours later, mice were subjected to a second recording session immediately following treatment with fluoxetine.

Elevated Plus Maze (EPM)

The EPM assay is widely employed to measure anxiety behavior in mice[54]. The following procedure was utilized for all studies except for the experiments conducted in unimplanted ClockΔ19 mice and their littermate controls. The EPM is comprised of four arms arranged in a cross shape, each measuring 30.5cm in length and 30.5cm in width, positioned at a height of 91.4cm from the floor. Additionally, there is a central region measuring 5cm by 5cm. Among the arms, two are designated as 'closed,' enclosed by walls that are 16.5cm in height on three sides, while the other two are 'open' and surrounded by a low piece of tape, approximately 1mm in height.

Two days prior to testing, mice were gently handled in the experimental room for roughly 1 minute per animal. Following gentle handling, mice were habituated to the room for 1 hour in a testing ‘home cage’.

936 Afterwards, mice were returned to group housing in their original home cage. This procedure was
937 repeated one day prior to experimental testing. On the testing day, mice were habituated to the
938 experimental room in their individual testing home cage for one hour. Mice were then connected to the
939 recording system and habituated for an additional 10 minutes. Following 5 minutes of neural and video
940 recordings from an overhead camera, mice were placed in the center of the EPM facing one of the
941 closed arms. Neural recordings and video data were acquired for an additional 5-10 minutes. Testing was
942 performed at 175 lux, during the light cycle. A subset of the mice (N=15) utilized to train and test the
943 multi assay model were previously used in a prior study to identify an electrode network that encoded
944 social appetitive behavior[26]. In that study, mice were recorded during social exploration, and activity in
945 the discovered network was also evaluated as mice explored an EPM.

946 For experiments conducted in unimplanted ClockΔ19 mice and their littermate controls, adult male and
947 female ClockΔ19 and WT mice (8-14 weeks; N=17 per genotype) were habituated to the testing room for
948 1 hour prior to testing. Chambers were cleaned with 70% ethanol and allowed to dry between animals.
949 The elevated plus maze (EPM) consisted of two plastic open arms perpendicular to two closed arms (30 ×
950 5 cm) and was elevated above the ground (60 cm). Mice were placed in the center of an EPM, and
951 behavior was recorded for 10 minutes. Ethovision video tracking software (Ethovision, Noldus, Leesburg,
952 VA, USA) was used to quantify the time spent in the open and closed arms, the number of entries into
953 the arms, and this distance travelled. Manual scoring was also conducted for verification. Testing was
954 performed at 20 lux.

955 **Bright Open Field (BOF)**

956 The bright open field assay is also widely employed to measure anxiety behavior in mice[54]. This assay
957 consists of a square arena (46 cm x 46 cm x 30 cm), in which the innermost third (i.e., 'center zone') is
958 considered to be more anxiogenic zone than the outermost two thirds (i.e., 'periphery zone'). Mice were
959 habituated to the experimental room in an individual testing home cage using the same procedure
960 described for the EPM. On the testing day, mice were connected to the recording system and five
961 minutes of neural and video data (from an overhead camera) were acquired while mice were in their
962 individual testing home cage. Mice were then placed in the periphery of the BOF, and an additional five
963 minutes of neural and video data were acquired while mice freely explored the arena. Testing was
964 performed at 125 lux, during the light cycle.

965 **Heart rate monitoring**

966 Unimplanted mice (N=7-9 male mice per assay and 7-8 female mice per assay) were anesthetized using
967 1% isoflurane, and the hair around their neck region was removed from using potassium thioglycolate
968 (Nair Body Cream, Church & Dwight Co. Ewing, NJ). Awake mice were then habituated to the monitor
969 cuff using a small or extra-small CollarClip (Starr Life Science Corp) for 1 hour/day for 7 days in their
970 homecage environment. Additionally, the mice used for the FLX assay experiment were habituated to
971 daily IP injections using saline.

972 On testing day, the CollarClip sensor was placed around their neck and they were allowed to acclimate
973 for 45 minutes. Measurements were then collected using the MouseOx Plus (Starr Life Sciences Corp,
974 Oakmont, PA). For EPM and BOF, baseline data was collected for 5 minutes while mice were in their
975 homecage, and for five minutes while mice were subjected to the EPM or BOF. For the fluoxetine assay
976 injections, mice were first injected with saline and recorded for 1 hour. After at least 5 hours, mice were
977 injected again with fluoxetine (10 mg/kg, i.p.) and recorded for an additional hour. Data points less than
978 250bpm were attributed to movement artifact and removed from the data. Data was acquired at 1Hz,
979 and mean heart rate values were calculated for the low and high anxiety contexts for each assay. A one-

tailed t-test was used to evaluate whether heart rate was higher in the high anxiety context vs. the low anxiety context.

Sleep State Identification

We utilized data collected as part of a previous study[33]. In brief, eight mice were implanted with the same brain targets as described above as well as a wire placed in the trapezius muscle to acquire electromyography (EMG) data. Mice were singly housed, habituated to the recording room for 2 days, and neural data was then collected for 24 hours. EMG power (root mean squared of the spectral amplitude of 30–56Hz) and a ratio of prelimbic cortex activity (2–4.5 Hz/2–9 Hz) were used to classify 3 sleep-wake states based our previously published clustering approach in mice[55]. High EMG activity and low prelimbic cortex 2–4.5 Hz/2–9 Hz activity corresponded to awake, low EMG activity but high prelimbic cortex 2–4.5 Hz/2–9 Hz activity corresponding to NREM sleep, and low EMG activity and low prelimbic 2–4.5 Hz/2–9 Hz activity corresponding to REM sleep. Data that was not classified within one of these three states was classified as 'unlabeled' (See Fig. 4A).

Using this classified data, we selected large time intervals for which neural data was classified as waking or REM sleep. Specifically, waking intervals were defined by at least 30 seconds of waking labeled data with at least 5 minutes of >95% wake labels on both sides of the data segment (Fig. 4B, top). REM sleep intervals were defined by at least 60 consecutive seconds that were labeled as REM sleep (Fig. 4B, bottom). LFP data from these intervals were then projected into *EN-Anxiety* and EN-SocialAppetitive[26]. All animals were recorded from each of the brain regions that composed both networks.

Delayed sucrose reward apparatus

The task chamber was constructed from Lego Duplo pieces of varied color, shape, and size. The apparatus had approximate dimensions of 48cm wide x 35cm deep x 30cm tall, and each wall was visually distinct. A nose poke detector was in the center of each wall, placed 1cm above the floor. There was also an LED light directly above each nose poke detector. The chamber was also equipped with four fluid dispensers, which were calibrated to release 5µL of 10% sucrose directly into each nose poke detector. The reward for three of the ports was also flavored with pumpkin, almond, or orange oil. The location and reward type remained fixed throughout each phase of experimental testing for all animals. During the task, the chamber was illuminated to 30 lux. The system was also equipped with speakers and an audiometer, and reward cues were played at 68dB. Signals from the nose poke detectors, LED lights, fluid dispensers, and audiometer were digitized and stored in parallel with our neural recordings.

Delayed sucrose reward apparatus, training, and task

Delayed sucrose reward task was modeled after a prior test in which mice had to remain in a spatial location in order to receive a food reward [56,57].

The task chamber was constructed from Lego Duplo® pieces of varied color, shape, and size. The apparatus had approximate dimensions of 48cm wide x 35cm deep x 30cm tall, and each wall was visually distinct. A nose poke detector was in the center of each wall, placed 1cm above the floor. There was also an LED light directly above each nose poke detector. The chamber was also equipped with four fluid dispensers, which were calibrated to release 5µL of 10% sucrose directly into each nose poke detector. The reward for three of the ports were also flavored with pumpkin, almond, or orange oil. The location and reward type remained fixed throughout each phase of experimental testing for all animals. During the task, the chamber was illuminated to 30 lux. The system was also equipped with speakers and an audiometer, and reward cues were played at 68dB. Signals from the nose poke detectors, LED lights, fluid dispensers, and audiometer were digitized and stored in parallel with our neural recordings.

After 7-14 days of recovery from surgical implantation of electrodes targeting the same regions composing *EN-Anxiety*, mice (N=9 C57 male mice) were food-deprived to 90% of their free-feeding body weight. During a training session, a mouse was connected to a recording cable and placed in the task apparatus. The training procedure is as follows:

- Stage 1: On the first day of training, mice freely accessed the testing chamber for 60 minutes. Each poke into a nose poke detector triggered a 500ms tone at 4000Hz and 5µL of reward release directly into the poke detector. This stage was repeated over 2 days.
- Stage 2: On the third and fourth day of training, mice were placed into the recording chamber together with their cage mates, without a recording cable. Mice were then allowed to freely explore the recording chamber for 120 minutes.
- Stage 3: On the fifth day, mice resumed individual training, during which they advanced in task difficulty after meeting specific criteria.
    - 3a: Each detected poke activated a 500ms, 4000Hz tone and released a 5µL reward at the beginning of the tone.
    - 3b: Each detected poke activated a 500ms, 4000Hz tone and released a 5µL reward at the end of the tone.
    - 3c: Each detected poke activated a 500ms, 4000Hz tone and released a 5µL reward at the end of the tone if a mouse remained in the nose poke detector.
    - 3d: Each detected poke activated a 500ms, 4000Hz tone and released a 5µL reward one second after the start of the tone if a mouse remained in the nose poke detector.
    - 3e: Each detected poke activated a 500ms, 4000+387Hz tone, and a second 500ms 4000Hz tone, one second after the start of the first tone. A 5µL reward was released 1.5 seconds after the start of the first tone if a mouse remained in the nose poke detector.
    - 3f: Each detected poke activated a 500ms, 4000+387Hz tone, and a second 500ms 4000Hz tone, one second after the start of the first tone. A 5µL reward was released at 2 seconds after the start of the first tone if a mouse remained in the nose poke detector.
    - 3g: Each detected poke activated a 500ms, 4000+387+387Hz tone, and a second 500ms 4000+387Hz tone one second after the prior tone, and a final 500ms 4000Hz tone one second after the last tone. A 5µL reward was released 2.5 seconds after the start of the first tone if a mouse remained in the nose poke detector.
    - This training pattern continued until mice passed training with a 5-second delay. For these trials, successive trials, tones of decreasing frequency were played, one at the beginning of each second, and mice received reward if the poke hole was activated for the entire test interval.
- A mouse passed a training stage when it completed 120 rewarded pokes in one day, or 120 rewarded pokes in two consecutive days and the second day reward count was greater than or equal to the reward count of the first day. Mice regressed to a prior training stage if they failed to complete a stage after five days, or if they received fewer than twenty rewards during a session. The data utilized for our electrophysiological analysis was acquired from 9 male mice after they completed training at the 5-second delay.

Social Preference Assay

A previously published data set[26] was used to assess the impact of social interaction on *EN-Anxiety* activity here. Briefly, mice implanted with electrodes at the same brain coordinates utilized for this study (N=12 C57 mice) were allowed to explore a rectangular arena (61cm × 42.5cm × 22cm, L×W×H) for 10 minutes. Two clear plexiglass walls divided the area into two equal chambers. Each chamber contained a circular holding cage (8.3cm diameter and 12cm tall) containing either a novel object or a C3H target

mouse matched for sex and age. Data was collected across 6-10 testing sessions/mouse. Video data was tracked using Bonsai Visual Reactive Programming software, and network activity was analyzed for periods in which mice were within ~5cm of the novel object or target mouse. Six of the twelve experimental mice were subjected to the EPM assay after the social preference assay, and their data were included as part of the training/validation/testing data for the multi-assay network model.

Optogenetic Stimulation and behavioral testing

Mice were injected with AAV5-ChR2-eYFP into ventral hippocampus at 7 weeks old. After 8 weeks, mice were implanted with a fiberoptic cannula either targeting right lateral hypothalamus (LH: −1.95AP, 0.5ML, −4.75DV; N=13 C57 mice) or right basal amygdala (Amy: -1.7AP, 3.0ML, -4DV; N=18 C57 mice). Behavioral experiments (bright open field, real-time place preference) were conducted after 2 weeks of recovery; experimental details are listed below.

Bright Open Field testing

Mice were habituated to the experimental room and fiberoptic tethering for 2 days prior to testing. The BOF arena was used for testing, where the innermost third was designated as the center zone. The center area was illuminated to 600 lux. On the testing day, mice were connected to the fiberoptic patch cord and immediately placed into the open field. All mice were stimulated with yellow light (593.5nm, OEM Laser Systems, Model No. MGL-F-593.5/80mW, 20Hz, 5ms pulse, either 1mW for Amy or 5mW for LH) while they explored the BOF chamber for three minutes. Mice were then pseudorandomized to receive either blue (473nm wavelength, CrystaLaser, CL473-025-O, 5ms pulse, either 1mW for Amy or 5mW for LH) or yellow light and stimulated for the next three minutes. The location of mice was tracked using Ethovision XT17 (Noldus). Behavior during this second stimulation interval using a one-tailed t-test to test whether greater avoidance was observed during blue light stimulation.

Real-time Place Preference

One week after BOF testing, mice were pseudorandomly re-assigned to either a blue or yellow light group. A two-chamber arena (60cm x 42cm x 22cm) was used where one side was randomly assigned to be the stimulation side for each mouse. Mice were connected to the fiberoptic cable and placed into the arena for twenty minutes. Real-time tracking (Neuromotive, Blackrock Neurotech) was used to activate the lasers (at the same conditions utilized for the open field testing) when a mouse was detected on the stimulation side. Movement was tracked using Ethovision XT17 (Noldus) and % time on the stimulation side was analyzed using a one-tailed t-test to test whether greater avoidance was observed during blue light stimulation.

Optogenetic Stimulation and Electrical Recordings

We modeled previously published methods for targeting the ventral hippocampus → lateral hypothalamus circuit [20]. Specifically, mice were anesthetized with 1.5% isoflurane and placed in a stereotaxic device. A 33-gauge Hamilton syringe was used to infuse 0.5 µl of AAV5-ChR2-EYFP at a rate of 0.1 µl/min into right ventral hippocampus (-3.16mm AP, 3.3mm ML, -3.75mm DV from dura; N=11 mice). Eight weeks later, mice were implanted with recording electrodes using the procedure and brain targets described above ('Electrode Implantation Surgery'). These electrodes included a bundle that was used to target the right lateral hypothalamus (LH: −1.95AP, 0.5ML, −4.75DV). A 100µm diameter fiberoptic (Doric Lenses) fiberoptic cannula was built into the LH bundle with the tip situated 250µm above the tip of the LH microwires bundle [58,59]. *In vivo* recordings were conducted after 2 weeks of recovery. Mice were habituated to the experimental room/setup for the two days preceding experiments. As a control experiment, the same procedure was used to test the impact of ventral hippocampus → amygdala

stimulation, with the exception that the optrode was implanted to target right amygdala (Amy: -1.7AP, 3.0ML, -4DV; N=9 mice) instead of right lateral hypothalamus. We also utilized a light intensity of 1mW because our initial experiments utilizing a light intensity of 5mW induced electroencephalographic and myoclonic seizures.

Mice were connected to the recording system using a fiberoptic patch cable and a 32-channel M headstage, and then placed in a new 'testing' home cage for 1 hour. On testing day, mice were connected and placed in the same testing home cage. After 40 minutes of additional habituation, neural data was recorded for 20 minutes. Mice were then stimulated with blue or yellow light for 10 minutes. Light stimulation was delivered at 20Hz, 5mW, with 5ms pulses and verified using a power meter (Thorlabs, PM100D). Mice were pseudorandomized to stimulation with either blue (473nm wavelength, CrystaLaser, CL473-025-O) or yellow light (593.5nm, OEM Laser Systems, Model No. MGL-F-593.5/80mW).

One week later, mice were subjected to a second recording with the other laser, using the same protocol described above. Thus, each mouse was stimulated with blue and yellow in pseudorandomized order across the two sessions.

Fear Conditioning

Mice were implanted with electrodes as described above ('Electrode Implantation Surgery'; N=36 male C57 mice). Following a two-week recovery period, mice were trained in a classic cued fear conditioning paradigm during which an auditory tone (conditioned stimulus; CS) was paired with an aversive air puff (unconditioned stimulus, US). The CS consisted of a 30-second, 10 kHz, 80dB, continuous auditory tone that was generated using MATLAB. The US consisted of a 2-second, 40 PSI, air puff that was introduced through 4 pumps, one built into each of the testing chamber's walls. Mice were randomly assigned to 2 groups: conditioned (CS+; N=17) and control (CS-; N=19). Behavioral testing was conducted in two different behavioral contexts (context A and B). Context A was a 10"×10"×11" (L×W×H), striped chamber made of alternating black and white Legos®. Context B was a 6"×12×11" chamber, with walls consisting of mixed colored Legos. Context A had a smooth floor, while context B had a textured floor.

Prior to conditioning (Day 0), mice were habituated to the behavioral room for 2 hours. On Day 1, mice were connected to the recording system and placed into Context A for 2 minutes. The fear-conditioned group was exposed to 7 trials of the CS. The US was presented during the last 2 seconds of each tone, and there was a pseudorandom interstimulus interval ranging from 60-120 seconds. The control group was exposed to 7 trials of the CS without the US. Each group remained in Context A for 1 minute after the last trial concluded. Neural and video data were collected throughout the trials. We also collected a continuous signal corresponding to the onset and offset of the CS.

Mice were then exposed to a cued recall session on Day 3. Here, mice were connected to the recording system and placed into Context B. After 3 minutes, mice were presented with the CS tone continuously for 3 minutes. Neural and video data was recorded throughout this interval, and the freezing behavior was quantified using Ethovision X12 (Noldus, Wageningen, the Netherlands) to detect the percentage of time during the CS presentation that the animal did not move. A subset of the conditioned mice (N=5) was also exposed to an extinction protocol on Day 2, where mice were presented with the CS, but not the US, in Context A. Since our objective was to quantify neural responses to fear conditioning on Day 1, and exposure to the one-day extinction protocol had no impact on freezing behavior on Day 3 (t_{26}=0.11 and P=0.92 using two-tailed unpaired t-test), we pooled this subset into the CS+ group for the analyses presented in the text. All implanted mice were used for behavioral analysis. Three conditioned mice and two control mice were removed from neurophysiological analysis due to poor signal quality.

1156 **Electrophysiological analysis of ClockΔ19 mice**

1157 ClockΔ19 mice and their wild type littermate controls were implanted and recorded in the EPM assay as
1158 described above (22-23 mice/genotype, balanced across sex). Six mice had poor electrophysiological
1159 signal prior to testing and were thus completely removed from the study. Four mice had poor quality
1160 video recordings and were thus removed from behavioral analysis (17-18 per genotype, balanced across
1161 sex, were used for behavioral analysis). Two of these mice had poor electrode placements and were thus
1162 removed from subsequent video electrophysiological analysis. Thus, a total of 33 mice (16-17 per
1163 genotype) were used for EPM location based electrophysiological analyses. Since the start time of the
1164 EPM task was noted for each experiment, the four mice with poor video quality were included in the
1165 analysis of network activity induced by task exposure (home cage vs EPM across genotype).

1166 For the EPM location analysis, the center of mass for each mouse was identified using DeepLabCut[60].
1167 This center of mass was then used to label the location of 1 second data windows as the center, open
1168 arm, or closed arm based on which location they spent more than half of the second. These center of
1169 mass-based labels were utilized for the analysis of closed arm/safe zone network activity in EPM. We
1170 also scored the location of the recording headcaps of mice using Ethovision. Because of the reduced size
1171 of the center location, we used the 1-second data windows for which both the center of mass and the
1172 headcap-based locations were labeled as the center mice as the center of the maze. This approach
1173 ensured high specificity for the windows labeled as the center.

1174 **Chronic Social Defeat Stress (cSDS)**

1175 These methods parallel those described in our prior work [27,59]. Data for our electrophysiological and
1176 behavioral analyses were obtained from two different cohorts of implanted mice. Behavioral data on the
1177 EPM was assessed from mice implanted in a different set of brain regions than those used for this study.
1178 Neurophysiological recordings in the home cage were obtained from mice implanted in the same brain
1179 regions utilized in this study. Data from a subset of this latter group of mice were previously used in our
1180 published work [26].

1181 Six- to seven-week old male C57 mice (N=50) were implanted with electrodes as described above
1182 ('Electrode Implantation Surgery'). Stress experiments were initiated two weeks after surgical recovery.
1183 All mice were singly housed prior to being subjected to chronic social defeat stress (cSDS). We modeled
1184 our protocol after previously published work [43,47]. Implanted animals were pseudorandomly assigned to
1185 control (N=16) or stress groups (N=34), such that cagemates were distributed across groups. Singly
1186 housed male retired-breeder CD1 (Charles River) mice were used as resident aggressors for 10 days of
1187 social defeat. Briefly, mice in the stress group were exposed to CD1 aggressors for 5 mins and only
1188 removed early in the event of serious physical injury (which never happened for more than two stressed
1189 mice animals per 10 day social defeat). Defeats were run in dim light conditions (~40-50 Lux). After 5
1190 mins, C57 mice and CD1 aggressors were separated with a perforated divider for 24 hours. Control C57
1191 mice were housed with another C57 mouse in a similar cage apparatus. Their C57 cage mates were
1192 rotated each day. This process was repeated for a total of 10 days. Triage was performed on stressed
1193 animals following each day of defeat to check for and treat any wounds. After this check, the lights were
1194 turned off. Mice that exhibited significant injuries during social defeat stress were removed from post-
1195 stress analysis. Neural recordings were obtained from all control and stressed mice in their home cage
1196 one day following completion of the cSDS protocol. Mice were subjected to these recordings in their
1197 home cage, immediately followed by recordings during a forced interaction test. This assay has been
1198 previously described[27,59,61], and only data from the home cage recordings are utilized in the present
1199 study.

A choice social interaction test was used to categorize stressed mice as susceptible or resilient [42,43,59,61]. This assay was performed 2 days after the last social defeat session, during the dark cycle of each mouse. Testing was conducted in a room with two red lamps facing the ceiling (2-10 lux). All animals were habituated to the room for approximately two hours prior to the start of testing. Experiments were pseudorandomized and balanced to include alternating control and stressed mice spread throughout the duration of experiment. For each trial, the experimental mouse was placed in the center of an opaque white 18" x 18" box, with 18" high walls and a wire-mesh sub-chamber at the center of one wall for 150 seconds. Then a CD1 mouse (low/non-aggressive) was placed in the enclosed sub-chamber, and the C57 mouse was placed back in the box for 2 minutes and 30 seconds. Behavior was recorded for the entirety of each trial. Stressed mice that showed higher interaction time with the empty sub-chamber than the sub-chamber containing the CD1 mouse were defined as susceptible. Mice that showed higher interaction time with the sub-chamber containing the CD1 were defined as resilient. Between mice, all chambers were cleaned with Super Sani-Cloth germicidal disposable wipes (PDI, Orangeburg, NY) or 70% ethanol and dried with kimwipes. Data was analyzed using Noldus Ethovision version 15.

Mice subjected to cSDS and their non-stressed controls were tested in the EPM 12 days following the last social defeat session. Animals were tested during their dark cycle in a dark room with two red light lamps facing the ceiling (2-10 lux at the surface of the behavioral arena). Animals were acclimated to the room for >1 hour prior to starting experiments. For each trial, animals were placed in the center of the apparatus facing the same side and allowed to explore the maze for 5 minutes. Afterwards, the animal was removed from the apparatus and placed back into its home cage. The trials were pseudorandomized and balanced with alternation of control and stressed animals. After each session, the EPM was thoroughly cleaned with Super Sani-Cloth germicidal disposable wipes (PDI, Orangeburg, NY) and dried with kimwipes. Data was analyzed using Noldus Ethovision version 15.

Chronic Mild Unpredictable Stress

We modeled our chronic mild unpredictable stress protocol after previously published work [45,46]. C57 male mice (N=21) were implanted at age 7-9 weeks with electrodes to target the same brain regions utilized to learn the anxiety-related networks. Two weeks later, cages of mice were pseudorandomized into a stress or control group. Control mice were subjected to gentle handling twice a week. The stress group was exposed to 2 aversive experiences each day – one during the light cycle and one during the dark cycle – for eight weeks, as previously described [45]. The stressors were as follows:

- physical restraint – mice were placed in a ~50mL plastic cone (with openings for breathing on both ends) for 1 hr
- shaking – a cage of mice was placed on an orbital shaker for 1 hr at 60 rpm
- overnight illumination – mice were exposed to regular room light during the 12-hr dark cycle
- inverted light cycle – mice were exposed to dark-cycle room conditions during the light cycle and light conditions during the dark cycle
- tilted cage – cages were tilted at a 45° angle for 12 hrs
- strobe – mice were placed in a room with a strobe light during the dark cycle for 12 hrs
- wet bedding – cage bedding was saturated with water for 12 hrs
- soiled rat bedding – cage bedding was replaced with used rat cage bedding for 3 hrs
- cold exposure – mice were placed in a cold room (4°C) for 1 hr
- missing bedding –bedding was completely removed from the cage for 12 hrs
- food and water restriction – food and water were removed for 12 hrs during the dark cycle
- overcrowding – cage space was reduced by 50% for 12 hrs during the dark cycle

Stressors were presented in pseudorandomized order, solely ensuring that animals did not receive the same stressor two days in a row. Body weight was monitored once a week to ensure mice didn't lose more than 10% body weight during the stress proposal.

Model Selection and Training

Label Assignment for Training Datasets

To make use of supervised machine learning methods, per-sample anxiety state labels must be assigned for our training assays. For the acute FLX assay, we accounted for drug activation time and assigned all time points within the last 30 minutes of the 1-hour recording to either a heightened or lower anxiety state after mice received FLX or saline, respectively. For the EPM and BOF assays, anxiety states within the assay can be ambiguous. To prevent mislabeling of anxiety states in these assays, we assigned all time points for which mice are in the EPM or BOF as a heightened anxiety state. We then labeled recordings taken while the mice were in their home cage environment as a lower anxiety state. With this formulation, all three training assays had the same labeling nomenclature of heightened anxiety and lower anxiety states regardless of the anxiogenic assay, allowing for easy combination and comparison during model training.

Training and Test Splits

Once features had been extracted for the FLX, EPM, and BOF assays, the complete data from an individual mouse was placed into one of two groups of data: training data and test data. These splits were performed per mouse such that all its data were contained in the same group, including if an individual mouse had data from multiple assays. Splitting by mouse is critical as it prevents a machine learning model from simply learning the identity of a mouse in the training data to achieve inflated performance on holdout data[62]. The training data were used for model development, where many sets of hyperparameters and model formulation were tested through a cross-validation procedure. Test data were kept as true holdout data, which we did not observe or test our model on until the final model architecture was determined. Once final model parameters were determined through cross-validation, the full training data was used for a final training run, and the output was then tested on the true test (holdout) data. Training and test groups had: 13 and 9 mice respectively for the FLX assay; 26 and 11 mice respectively for the EPM assay; and 19 and 9 mice respectively for the BOF assay. 17 training mice and 7 test mice were shared across 2 assays (EPM and BOF). There was a single test mouse that was exposed to all three assays.

Discriminative Cross-Spectral Factor Analysis (dCSFA-NMF)

Discriminative Cross-Spectral Factor Analysis - Nonnegative Matrix Factorization (dCSFA-NMF) is a machine learning framework for discovering key predictive factors relevant to a behavioral assay or emotional state of interest [25]. This method has been used previously to detect brain networks corresponding to stress and social activity in mice using LFP data[26]. Similar to other factor models that have been used in neuroscience, such as principal component analysis (PCA), independent component analysis (ICA), and nonnegative matrix factorization (NMF), dCSFA-NMF identifies underlying components that are interpreted to be networks of connectivity. The superposition of these networks then explains the observed neural activity. While the previously mentioned unsupervised methods can identify networks of neural activity, it is unlikely that anxiety and other emotional states make up one of these dominant networks. Thus, dCSFA-NMF makes use of a supervision component to ensure that one or more of the learned networks are correlated with a behavioral measure or emotional state of interest,

meaning that it learns networks that both explain the observed neural activity and decode conditions of interest.

Rigorously, the model learns K fixed components $W \in \mathbb{R}^{K \times M}$ that can reconstruct observed data $X \in \mathbb{R}^{N \times M}$ using an array of network activity scores $s \in \mathbb{R}^{N \times K}$ such that $X = sW$. The observed data X are formed from the features extracted from the LFP signals (see "Feature Extraction" above), where each window of data $x_n \in \mathbb{R}^M$ represents the concatenation of power, coherence, and Granger causality features. W and s are constrained to be positive since the features of use – power, coherence, and Granger causality – observed in X are also nonnegative. Network activity scores are inferred from the observed data using an encoder function $s = f_\theta(X)$, which can take the form of a neural network or linear model. The activity scores $s_s \in \mathbb{R}^{N \times Q}$ of the $K \geq Q \geq 1$ supervised components are then used in a logistic regression model f_ϕ to predict the behavior of interest $y = f_\phi(s_s)$. We constrain our predictions to use a sparse combination of all networks, namely only the supervised networks, to narrow the scope of our network discovery and reduce the total number of comparisons. The parameters of the model are then optimized using the loss function,

$$\min_{W,\theta,\phi} \sum_{i=1}^{N} \mathcal{L}_x\big(x_i, W f_\theta(x_i)\big) + \lambda \mathcal{L}_y\left(y_i, f_\phi\big(f_\theta(x_i)\big)\right) + \alpha \mathcal{L}_{w_s}\big(x_i, W f_\theta(x_i)\big).$$

Here, $\mathcal{L}_x$ is the reconstruction error between the original power, coherence, and Granger directionality features and those features generated by the product of our network scores and networks, sW. In this work, we make use of the Mean-Squared-Error (MSE) function. Our predictive loss $\mathcal{L}_y$ is a binary cross-entropy loss and penalizes our model for incorrectly predicting the behavioral state of each window. The impact of the predictive loss can be tuned using the hyperparameter λ. Lastly, we impose a second reconstruction loss, $\mathcal{L}_{w_s}$, on the supervised network scores. This reconstruction loss prevents our neural network encoder f_θ from learning an uninterpretable near-zero noise embedding for the supervised scores, which predicts the condition of interest (e.g., which condition of an anxiety assay a mouse is in) well with little to no contribution to explaining neural activity. This loss can be formulated as another MSE loss between the outer product of the supervised network activations and the supervised electome network and the features. Alternatively, this loss can be formulated as a penalty to drive the supervised network scores to reconstruct the residual of the unsupervised networks and features. We used the latter in our analysis.

Performance Metrics – Predictive Modeling

To evaluate the predictive performance of our model, we used the receiver operating characteristic curve - area under the curve (ROC-AUC). This metric is common in machine learning literature and is closely related to the concordance index for evaluating discrimination between binary labels. In our setting, the binary labels correspond to periods classified as a heightened anxiety state versus a lower anxiety state (e.g., elevated plus maze vs home cage in the behavioral assays). AUC is a rank-based metric that quantifies the probability that a randomly chosen heightened-anxiety period receives a higher summary value than a randomly chosen lower-anxiety period. AUC has values in the range [0,1] where AUC=0.5 indicates chance level discrimination. AUC=1 perfect separation of the two binary states, and AUC=0 indicates perfect separation with the label ordering reversed. That is, the summary values used in the metric are consistently ordered such that lower-anxiety periods receive higher values than heightened-anxiety period. AUC is evaluated using a Mann-Whitney-U statistical test.

For evaluating our models, we obtained an AUC for each mouse (e.g., how well does the model discriminate between a heightened anxiety state versus a lower anxiety state) and then reported the

data group mean and standard error of the mean for each assay (e.g., FLX, EPM, BOF). Reporting AUC for each mouse rather than one single AUC value over all windows is more reflective of discriminative ability due to the differencing base anxiety levels between mice. Additionally, many of our behavioral contexts have varying neural recording lengths; by reporting AUC values for each mouse separately, we addressed the possibility of our model overfitting to the neural activity of mice in paradigms with longer recordings and therefore more samples.

Performance Metrics – Generative Modeling

We evaluated how well our models explained neural activity in the brain by quantifying the mean-squared-error (MSE) of the model's predicted power, coherence, and Granger directionality features and the originally observed values.

$$MSE(x, \hat{x}) = \frac{1}{N}\sum_{n=1}^{N}(x_n - \hat{x}_n)^2$$

During model training, we weighted the reconstruction of each of our feature types (power, coherence, Granger directionality) by their prevalence, such that power holds equal importance to coherence and Granger directionality despite representing a smaller number of power features.

Performance Metrics – Model Consistency

In addition to our ability to reconstruct neural data and discriminate anxiety levels, we want our networks to be reliable and consistent, in the sense that they would be robust to minor perturbations of the data. Therefore, we measured how similar our electome networks of interest (the learned values of W corresponding that are predictive) are when learned from slightly different subsets of training data, which we refer to as "representation consistency.[63]"

To evaluate representation consistency in our model, we created a representation consistency distance score based on the weighted average cosine distance formula between vector representations of electome networks. Cosine distance calculates the angular separation between two vectors and takes values in $[0,1]$ for nonnegative vectors, where 0 represents perfect alignment and 1 represents orthogonal vectors. The cosine distance between two vectors, A and B is given by:

$$\mathcal{D}(A, B) = 1 - \frac{A \cdot B}{\|A\|\|B\|}$$

During the training process, we independently learned model parameters on two subsets of data (described below). After learning, we matched networks between each set of data to determine how similar the network in the first subset of data is to its uniquely matched network in the second subset of data, with details given in the next paragraph. Instead of averaging directly over resultant cosine distances, we chose to weight each unique pairing in the average by the impact that a network score had on the prediction relative to the other networks. In other words, a network that does much of the prediction on whether an animal is in a higher or lower anxiety state will be weighted higher in the average representational consistency. A consistent representation or network discovery method will yield a low distance score, as networks that are exactly the same would receive a value of 0, whereas completely orthogonal networks would receive a value of 1.

To determine the optimal matching, we first calculate the cosine distance of all potential pairwise matches between supervised networks from each set of data. We then use the Hungarian Matching Algorithm [64] to determine the unique pairwise matching that minimizes the average cosine distance,

meaning that each supervised network learned on the first set of data has a unique match to a supervised network learned on the second set of data. In other words, if network 1 from the first set of data is very similar to network 2 from the second set of data, those networks would be matched as they would have a low cosine distance.

Single-assay Model Formulation and Training

For single-assay model training, we isolated one of our three training assays (EPM, BOF, FLX) to use as our training dataset for dCSFA-NMF. While we focused on our model training using the FLX assay in the results section, we also trained models using the EPM and the BOF as singular training datasets. Each of our three single-assay models used the same labeling structure outlined above (see *"Distributed electome networks encode a convergent anxious internal state"*).

These models were learned using 4-fold cross validation on the training data. Models were selected based on predictive performance. Predictive performance was evaluated on the concatenated training and validation partitions of the other two assays not used for model training. It is worth noting that some bias exists in this evaluation, as some mice in the other two assays also experienced the third assay and their data may have been present in the training set of the selected model-training assay. However, even with this bias, these models failed to generalize across assays. The test, or holdout, partitions of all three assays were left untouched as each of the single-assay models failed to generalize to all three assays.

We performed our single-assay model training twice. First, we trained the models using a single supervised network[26]. Second, after we identified the value of multi-assay training and tuning for multiple consistent predictive networks, we reperformed our single-assay training with three supervised networks (as was selected in the multi-assay model below) and 27 unsupervised networks to allow for the most similar comparison with the multi-assay model. This second round of training was important as we wished to properly attribute whether generalization improvements from the multi-assay model came from increased model capacity or were due to the multi-assay training procedure.

Multi-Assay Model Formulation and Training

As mentioned above, our multi-assay model formulation involves concatenating the EPM, FLX, and BOF training datasets into a single training dataset. As the labels for each assay are distilled into heightened anxiety and lower anxiety states depending on the assay of interest, data concatenation is possible as the labels are consistent. For multi-assay model training, we performed 4-fold cross validation on the training data partitions of all three assays for hyperparameter tuning. As mentioned earlier ('Training and Test Splits' section), all the data for a mouse is constrained to be completely with a training or validation fold, which is also known as a group K-fold cross-validation, where the mouse identity is used to as the group. We then select model parameters based on the strategy described below in the "Hyperparameter Selection Strategy" section. The final model is learned on all training data with the selected hyperparameters, which is then used to evaluate on the test data.

Hyperparameter Selection Strategy

The dCSFA-NMF model requires selection of several hyperparameters. These factors include the number of electome factors K, number of supervised networks Q, the importance of the supervised task λ, and the importance of the supervised factor reconstruction α. These terms all impact the model learned as described in the "*Discriminative Cross-Spectral Factor Analysis (dCSFA-NMF)*" section. The number of electome factors K control how well we can reconstruct the original LFP data. The number of supervised electome factors Q impacts how well we can decode our anxiety states and our representational

consistency. High representational consistency indicates that the same underlying network structure is reliably recovered across training perturbations, which is essential for interpreting the learned electome networks as stable, biologically meaningful circuits rather than dataset-specific solutions. In other words, across plausible data perturbations, the same circuit-level structure is repeatedly recovered. High representational consistency is required for downstream experimental design because causal perturbations necessarily target specific circuit features; without a stable network structure, experimental outcomes would be ambiguous, as null results could reflect instability of the learned representation rather than a true lack of biological relevance. Identifying a suitable number of supervised networks is especially crucial in the case where multiple underlying networks may be driving the emotional or behavioral state. Underspecifying the number of supervised networks to learn may result in the model inconsistently swapping across a subset of these suitable underlying networks.

We defined the encoder $f_\theta(X)$ as a small neural network; specifically it was a multi-layer perceptron with a single hidden layer of size 256 with a leaky rectified linear unit after the first hidden layer and a softplus nonlinearity before the output to maintain positivity of our network scores. We set $\lambda = \alpha = 1$, and found performance of our model was robust to changes in the network definition and those hyperparameters.

To choose the value of K, we first performed 4-fold cross-validation-over-subjects for $K = \{2,4, \dots ,58\}$ while limiting the number of supervised networks $Q = 1$. Each model was trained on the training mice for all three assays jointly and evaluated on the validation mice for all assays, as per the multi-assay training procedure. We observed that the predictive performance of all three assays stabilized at K = 18 with little change across all three assays for higher values (Supplemental Fig. S5A). Subsequently, we found that the reconstruction performance plateaued at K = 30. Given that the predictive performance was consistent for K > 18, we selected K = 30 as the total number of networks that our model would learn. We evaluated this pattern for different values of Q and found the same patterns.

To choose a value of Q, we aimed to balance 3 design priorities in our model formation. First, our model must be predictive of the behavior of interest. Second, our model should find a relatively consistent solution (i.e. discovered brain networks should be similar across multiple runs), as this is necessary to have confidence in the networks and downstream experiments based on them. Lastly, our solution should be simple. Suppose we were to supervise all the networks in our model. We likely would achieve strong predictive performance; however, multiple-hypothesis testing problems would arise as we begin to test the relationships of each network with behavior. Therefore, we wished to find a stable, predictive solution that makes use of the smallest Q of supervised networks possible. To ascertain the value of Q we should use, we learned models with values $Q = \{1,2,3,4,5,10,20\}$ with $K = 30$ using 4-fold cross-validation-over-subjects. We calculated the predictive performance on our anxiety assays and evaluated the average consistency score between the folds. The number of supervised networks does not greatly affect the overall prediction quality (Supplemental Fig. S5B, left), however, increasing the total number of supervised networks can significantly improve the representational consistency of the behaviorally relevant networks discovered (Supplemental Fig. S5B, right). We observed that the average AUC across all three assays peaks around $Q \in \{3,4\}$ and declined slightly as the number of supervised networks further increased, as shown in Supplemental Fig. S5A.

Additionally, we constrained our model to only identify supervised networks with scores that positively correlated with predicting a heightened anxiety state, as we aimed to discover an anxiety network indicative of higher anxiety states rather than an anxiety inhibition network.

To learn the models, we first pretrained our factors by training a traditional nonnegative matrix factorization model (NMF) on our data. We selected stochastic gradient descent as our optimization

algorithm as it is known to offer better generalization performance despite requiring longer training times [65]. We used a learning rate of .001 and a momentum value of .9.

Our datasets were imbalanced with the longer-duration FLX neural recordings making up a much higher percentage of our total data. Therefore, we resampled windows from EPM and BOF such that each experimental context was equally influential on our network pretraining. We then froze the weights of our sorted NMF factors and trained the encoder to learn scores corresponding to the fixed factors and the classifier to predict corresponding labels (e.g., higher and lower anxiety states) based on those scores. We found that training the encoder and classifier for 500 epochs of neural recording data (e.g., 500 passes over all training data) was sufficient for the optimization algorithm to converge and stabilize at a minimum of the loss function. After pretraining, we then unfroze all parameters and trained them jointly. We found that an additional 500 epochs were sufficient for the model training to converge and stabilize at a minimum of the loss function.

Model Validation

Networks Decoded Assays Jointly

Given that our dCSFA-NMF model selection procedure identified three separate networks (see "*Hyperparameter Selection Strategy*"), we wished to validate that each of the learned networks are not simply learning to predict for each of the three training assays independently. Networks that truly capture anxiety should not be relevant to only one context where anxiety may be experienced but should generalize to multiple contexts. Here, we evaluated the per-mouse AUC for each of the networks separately using the Mann-Whitney-U test in each of the three training assays (Fig. 2D).

Individual Network Contribution Towards Prediction

We also considered whether one or more of our networks may not have contributed substantially to the overall prediction of the mouse's internal anxiety state. To evaluate this, we considered the mean prediction logit of each network given by the mean network score multiplied by its corresponding logistic regression coefficient and normalized it by the sum the mean prediction logits of all supervised networks. More formally, we defined the mean logit of an individual network as $z_j = \bar{s}_j \phi_j$, where $\bar{s}_j$ is the mean network activity score from the holdout data for network j , and ϕ_j is the dCSFA logistic regression coefficient corresponding to that network activity score. Since we constrained our network to have positive network activity scores and logistic regression coefficients, no absolute value or squaring of the logits was necessary for comparison. We then evaluated the contribution of each network j as:

$$Contribution(j) = \frac{z_j}{\sum_{i=1}^{K} z_i}$$

This metric quantified the average predictive impact of each network on the prediction using holdout data.

Detailed Methods for validation analyses

<u>Location-based dynamics in network activity</u>

To compare post-exposure effects for the safe and avoidance zones in the EPM/BOF on *EN-Anxiety* dynamics, we extracted data from each timepoint in each location. We also extracted data in the five seconds preceding and following these timepoints. Here, the locations of C57 mice (closed arm/open arm/center for EPM and center/periphery for BOF) were encoded using Ethovision on 50 frames-per-second video recordings of the task, tracked at 25fps based on their center of mass. Frame labels were

then aligned with our one-second resolution LFP features by assigning the label of each 1-s window that made up most of the Ethovision frames for that timepoint. For example, a time window was labeled as open arm if 20% of the Ethovision frames corresponded with the open arm location.

We then determined the *EN-Anxiety* activity at all instantaneous timepoints where the mouse was in the region of interest and at all observed timepoints within a +/- 5 second window from the instantaneous timepoint. Timepoints for which electrophysiological data, and therefore network scores, were not observed due to electrophysiological artifact, were dropped. For each mouse, network activity was averaged within the -5 to -1s window, the 1s to 5s window, and the instantaneous timepoint window. Activity was then normalized compared to home cage and compared between locations across mice.

Fluoxetine Network Dynamics

We validated our network's ability to decode anxiety attenuation post-injection with saline or fluoxetine in the holdout mice from the FLX training task. Nine mice were injected with saline or fluoxetine at t=0 and we recorded neural activity for one-hour post-injection. We then observed *EN-Anxiety* activity during the full hour recording for the 9 holdout mice. Network activity scores were binned and averaged at a 5-minute resolution with the mean and standard error activity across mouse plotted in Fig. 3A. It is worth restating that our model was trained only using timepoints during the second half of the one hour-long recorded data to ensure full absorption of the injected fluoxetine and to minimize handing effects. While our model was biased to distinguish between fluoxetine and saline due to our model training task, the model had no prior exposure to timepoints between t= [0,30] mins and no explicitly supervised trend for those timepoints. Data were analyzed using a two-way repeated measures ANOVA.

Delayed sucrose reward task

We examined *EN-Anxiety* activity during the delayed sucrose reward assay to validate that *EN-Anxiety* was not encoding reward or arousal. Pump events for delivering sucrose to the mice were much shorter than our one-second windows, therefore we used the event-triggered feature extraction code to precisely extract one second windows surrounding an event (sucrose delivery). We collected LFP features for 4 seconds prior to and 4 seconds after the pump event. These features were then projected into *EN-Anxiety*. Mean network activity at one second prior and one-second post-pump event were then compared across mice (n=8) using a one-tailed Wilcoxon signed rank test.

Optogenetic Stimulation of Ventral Hippocampus Circuits

We quantified network activity during optogenetic stimulation of the ventral hippocampus to lateral hypothalamus circuit and a control ventral hippocampus to amygdala circuit. We previously demonstrated that in the absence of ChR2, blue light stimulation has no direct impact on LFP activity using our recording approach[58]. Moreover, yellow light stimulation has no direct impact on LFP activity in the presence of ChR2[26,50]. Thus, we chose to compare network activity during yellow light stimulation and blue light stimulation, which all animals received. This approach enabled us to perform within-subject comparisons.

Fear Conditioning

For *EN-Anxiety* validation, event-centered features were extracted for 10 seconds prior to the tone and 20 seconds after the tone onset. Mean *EN-Anxiety* activity was then calculated for the control and conditioned mice for both the 10 seconds pre-segment and the 20 seconds post-segment separately. For both segments, we utilized a repeated measures two-way ANOVA to determine the impact of the 7th and final tone/air puff event within and between groups. We isolated the 7th event under the assumption

that the conditioned mice had successfully associated the tone stimulus with the air puff across the 6 prior trials. For analyzing the response of *EN-Anxiety* during the air puff, we only utilized mice for which network activity could be isolated for the complete 2 seconds of the air puff (7/13 CS+ mice and 15/17 CS- mice).

Statistical Analysis Philosophy

We trained a multi-region, multi-assay model to putatively encode the anxiety state. We also trained models to test whether this putative state was encoded by single regions and/or by pairs of brain regions. We assessed each single-region or paired-region model independently for the three assays. Based on our prior observations that other emotional internal states could not be decoded from individual brain regions [26,27,51], we hypothesized that activity from single regions and/or pairs of regions would fail to decode a convergent anxiety state as well. To increase the likelihood of falsifying our hypothesis we chose to leave all our statistical analysis using single region/pairs of regions uncorrected. We observed that P>0.05 for at least one assay for each single region/pairs of regions test. Since correcting for multiple comparisons would have served to further increase the P-values, we concluded that no single region/pairs of regions encoded a convergent anxiety state.

Next, to validate the multi-region, multi-assay networks, we recorded LFP data in the same brain regions from new mice and/or new paradigms. We focused this subsequent analysis on Electome Network 2/*EN-Anxiety* since this network independently encoded all three of our initial anxiety assays, it showed highest contribution to the joint predictive model, and this network did not represent a superposition of the FLX and BOF/EPM assays. Validation of *EN-Anxiety* involved various statistical tests and procedures. For comparison of high anxiety vs. low anxiety conditions, we performed non-parametric statistical tests on mean network scores for intervals or groups of interest. In cases where parametric tests are useful, such as examining network dynamics over time, we performed a Box–Cox transformation of the network activity scores prior to statistical testing. For the validation tests, we expected the activity of *EN-Anxiety* to be higher in the high anxiety condition compared to the low anxiety condition since the learned model matched higher network activity to the higher anxiety contexts. For these cases, we performed statistical tests with a one-tailed test. A similar approach was implemented for our control experiments. Specifically, we tested whether network activity responded in the same manner to other psychological constructs including arousal and rewards as it had to anxiety.

We hypothesized that anxiety-related behavior and network activity would be lower in the *ClockΔ19* mouse model of mania. Thus, we utilized a one-tailed test for behavior. We utilized a two-way ANOVA to analyze network activity since we were testing both the impact of genotype and expose to the EPM assay. All such cases are disclosed in our results section. All p-values are reported as uncorrected p-values network analyses.

In some cases, such as examining network dynamics in the safe regions over time (Fig. 3B), missing observations cannot be determined to be missing completely at random. Therefore, in such cases, we make use of an ANCOVA analysis strategy, which is flexible with missing data and allows analysis of dynamics over time. A disadvantage of this approach is that samples are treated independently without concern of subject identity.

Visualization

Networks were visualized as chord plots using code adapted from https://github.com/carlson-lab/lpne/ to allow for recoloring of frequency bands. Significant features were determined by calculating the average percent contribution of each network towards the reconstruction of each feature for the training task holdout mice. This strategy results in an even appraisal of low and high frequency features, even

though low frequency spectral features tend to have higher power. We then selected the 85th percentile of these contributions, which is a threshold that adequately highlights dominant features without cluttering the plot and is consistent with related works [26]. Finally, these features were plotted with a transparency ranging from 40 to 90% based on their strength with each network.

Reproducibility

Computational Environment and Codebase Disclosure

Preprocessing and feature extraction code was performed in MATLAB R2022a using the LFP feature extraction pipeline found on the main branch at https://github.com/carlson-lab/lpne-data-analysis. Event-triggered feature extraction code can be found on the "framewindows" branch of the same repository. A PyTorch implementation of dCSFA-NMF can be found at https://github.com/carlson-lab/lpne/. All code for network generation, hyperparameter tuning, model implementation, plotting, and a singularity definition file for replicating our Python environment can be found https://github.com/carlson-lab/Anxiety. Development was performed on a computer cluster in a Singularity Container managed Python environment with nodes utilizing an NVIDIA RTX 2080 Ti.

Author Contributions – Conceptualization DNH, MHK, RCH, SDM, DEC and KD; Methodology, DNH, MHK, WEC, DEC, and KD; Formal Analysis, DNH, MHK, KKWC, GET, YG, YF, MT, and KD; Investigation, DNH, MHK, KKWC, GET, YG, DW, AM, YF, MT, AF, NMG, and KD; Resources, CAM, RCH, DEC and KD; Writing – Original Draft, DNH, MHK, JMZ, DEC, and KD; Writing – Review & Editing, DNH, MHK, KKWC, CAM, JMZ, RH, SDM, DEC, and KD; Visualization, DNH, MHK, DEC, and KD; Supervision, CAM, RCH, DEC and KD; Project Administration, DEC and KD; and Funding Acquisition, DNH, RCH, DEC, and KD; (see Supplemental Table S1 for experiment specific contributions).

Declaration of Interests

The authors have no competing financial interests.

Acknowledgements

We would like to thank Elise Adamson, Jake Benton, and Rachel Fisher-Foye for technical assistance, and Karim Abdelaal for comments. This work was supported by Hope for Depression Research Foundation, and NIH Grants 1R01MH099192, R01MH120158, and 1DP1MH132709 to KD. A special thanks to Freeman Hrabowski, Robert and Jane Meyerhoff, and the Meyerhoff Scholarship Program.

References

1 Szuhany, K. L. & Simon, N. M. Anxiety Disorders: A Review. *JAMA* **328**, 2431-2445 (2022). https://doi.org/10.1001/jama.2022.22744

2 Ruscio, A. M. *et al.* Cross-sectional Comparison of the Epidemiology of DSM-5 Generalized Anxiety Disorder Across the Globe. *JAMA psychiatry* **74**, 465-475 (2017). https://doi.org/10.1001/jamapsychiatry.2017.0056

3 Czeisler, M. E. *et al.* Mental Health, Substance Use, and Suicidal Ideation During the COVID-19 Pandemic - United States, June 24-30, 2020. *MMWR Morb Mortal Wkly Rep* **69**, 1049-1057 (2020). https://doi.org/10.15585/mmwr.mm6932a1

4 Taylor, J. M. & Whalen, P. J. Neuroimaging and Anxiety: the Neural Substrates of Pathological and Non-pathological Anxiety. *Curr Psychiatry Rep* **17**, 49 (2015). https://doi.org/10.1007/s11920-015-0586-9

5 Robinson, O. J., Pike, A. C., Cornwell, B. & Grillon, C. The translational neural circuitry of anxiety. *J Neurol Neurosurg Psychiatry* **90**, 1353-1360 (2019). https://doi.org/10.1136/jnnp-2019-321400

6 Takagi, Y. *et al.* A common brain network among state, trait, and pathological anxiety from whole-brain functional connectivity. *NeuroImage* **172**, 506-516 (2018). https://doi.org/10.1016/j.neuroimage.2018.01.080

7 Lai, C. H. Task MRI-Based Functional Brain Network of Anxiety. *Advances in experimental medicine and biology* **1191**, 3-20 (2020). https://doi.org/10.1007/978-981-32-9705-0_1

8 Kirkby, L. *et al.* An amygdala-hippocampus subnetwork that encodes variations in human mood. *Cell* **In press** (2018).

9 Moreira, C. M., Masson, S., Carvalho, M. C. & Brandao, M. L. Exploratory behaviour of rats in the elevated plus-maze is differentially sensitive to inactivation of the basolateral and central amygdaloid nuclei. *Brain Res Bull* **71**, 466-474 (2007). https://doi.org/10.1016/j.brainresbull.2006.10.004

10 Ciocchi, S. *et al.* Encoding of conditioned fear in central amygdala inhibitory circuits. *Nature* **468**, 277-282 (2010). https://doi.org/10.1038/nature09559

11 Calhoon, G. G. & Tye, K. M. Resolving the neural circuits of anxiety. *Nat Neurosci* **18**, 1394-1404 (2015). https://doi.org/10.1038/nn.4101

12 Adhikari, A., Topiwala, M. A. & Gordon, J. A. Synchronized Activity between the Ventral Hippocampus and the Medial Prefrontal Cortex during Anxiety. *Neuron* **65**, 257-269 (2010).

13 Adhikari, A., Topiwala, M. A. & Gordon, J. A. Single units in the medial prefrontal cortex with anxiety-related firing patterns are preferentially influenced by ventral hippocampal activity. *Neuron* **71**, 898-910 (2011). https://doi.org/10.1016/j.neuron.2011.07.027

14 Seidenbecher, T., Laxmi, T. R., Stork, O. & Pape, H. C. Amygdalar and hippocampal theta rhythm synchronization during fear memory retrieval. *Science* **301**, 846-850 (2003).

15 Dzirasa, K. *et al.* Impaired limbic gamma oscillatory synchrony during anxiety-related behavior in a genetic mouse model of bipolar mania. *J Neurosci* **31**, 6449-6456 (2011). https://doi.org/10.1523/JNEUROSCI.6144-10.2011

16 Lee, A. T. *et al.* VIP Interneurons Contribute to Avoidance Behavior by Regulating Information Flow across Hippocampal-Prefrontal Networks. *Neuron* **102**, 1223-1234 e1224 (2019). https://doi.org/10.1016/j.neuron.2019.04.001

17 Jacinto, L. R., Cerqueira, J. J. & Sousa, N. Patterns of Theta Activity in Limbic Anxiety Circuit Preceding Exploratory Behavior in Approach-Avoidance Conflict. *Frontiers in behavioral neuroscience* **10**, 171 (2016). https://doi.org/10.3389/fnbeh.2016.00171

18 Felix-Ortiz, A. C. *et al.* BLA to vHPC inputs modulate anxiety-related behaviors. *Neuron* **79**, 658-664 (2013). https://doi.org/10.1016/j.neuron.2013.06.016

19 Felix-Ortiz, A. C., Burgos-Robles, A., Bhagat, N. D., Leppla, C. A. & Tye, K. M. Bidirectional modulation of anxiety-related and social behaviors by amygdala projections to the medial prefrontal cortex. *Neuroscience* **321**, 197-209 (2016). https://doi.org/10.1016/j.neuroscience.2015.07.041

20 Jimenez, J. C. *et al.* Anxiety Cells in a Hippocampal-Hypothalamic Circuit. *Neuron* **97**, 670-683 e676 (2018). https://doi.org/10.1016/j.neuron.2018.01.016

21 Kjaerby, C., Athilingam, J., Robinson, S. E., Iafrati, J. & Sohal, V. S. Serotonin 1B Receptors Regulate Prefrontal Function by Gating Callosal and Hippocampal Inputs. *Cell Rep* **17**, 2882-2890 (2016). https://doi.org/10.1016/j.celrep.2016.11.036

22 Padilla-Coreano, N. *et al.* Direct Ventral Hippocampal-Prefrontal Input Is Required for Anxiety-Related Neural Activity and Behavior. *Neuron* **89**, 857-866 (2016). https://doi.org/10.1016/j.neuron.2016.01.011

23 Padilla-Coreano, N. *et al.* Hippocampal-Prefrontal Theta Transmission Regulates Avoidance Behavior. *Neuron* **104**, 601-610 e604 (2019). https://doi.org/10.1016/j.neuron.2019.08.006
24 Walder-Christensen, K. *et al.* Electome network factors: Capturing emotional brain networks related to health and disease. *Cell Rep Methods* **4**, 100691 (2024). https://doi.org/10.1016/j.crmeth.2023.100691
25 Talbot, A., Dunson, D., Dzirasa, K. & Carlson, D. Estimating a brain network predictive of stress and genotype with supervised autoencoders. *J R Stat Soc Ser C Appl Stat* **72**, 912-936 (2023). https://doi.org/10.1093/jrsssc/qlad035
26 Mague, S. D. *et al.* Brain-wide electrical dynamics encode individual appetitive social behavior. *Neuron* **110**, 1728-1741 e1727 (2022). https://doi.org/10.1016/j.neuron.2022.02.016
27 Hultman, R. *et al.* Brain-wide Electrical Spatiotemporal Dynamics Encode Depression Vulnerability. *Cell* **173**, 166-180 e114 (2018). https://doi.org/10.1016/j.cell.2018.02.012
28 Marcinkiewcz, C. A. *et al.* Serotonin engages an anxiety and fear-promoting circuit in the extended amygdala. *Nature* **537**, 97-101 (2016). https://doi.org/10.1038/nature19318
29 Cunniff, M. M., Markenscoff-Papadimitriou, E., Ostrowski, J., Rubenstein, J. L. & Sohal, V. S. Altered hippocampal-prefrontal communication during anxiety-related avoidance in mice deficient for the autism-associated gene Pogz. *Elife* **9** (2020). https://doi.org/10.7554/eLife.54835
30 Caruana, R. Multitask Learning. *Machine Learning* **28**, 41–75 (1997).
31 Jackson, A. D. *et al.* Amygdala-hippocampus somatostatin interneuron beta-synchrony underlies a cross-species biomarker of emotional state. *Neuron* **112**, 1182-1195 e1185 (2024). https://doi.org/10.1016/j.neuron.2023.12.017
32 Berg, L., Eckardt, J. & Masseck, O. A. Enhanced activity of pyramidal neurons in the infralimbic cortex drives anxiety behavior. *PLoS One* **14**, e0210949 (2019). https://doi.org/10.1371/journal.pone.0210949
33 Walder-Christensen, K. K. *et al.* Sleep-wake states are encoded across emotion-regulation regions of the mouse brain. *eNeuro* (2025). https://doi.org/10.1523/ENEURO.0291-25.2025
34 Gunaydin, L. A. *et al.* Natural neural projection dynamics underlying social behavior. *Cell* **157**, 1535-1551 (2014). https://doi.org/10.1016/j.cell.2014.05.017
35 Maestas-Olguin, C., Fennelly, J. W. & Pentkowski, N. S. Chemogenetic inhibition of ventral hippocampal CaMKIIalpha-expressing neurons attenuates anxiety- but not fear-like defensive behaviors in male Long-Evans hooded rats. *Neurosci Lett* **751**, 135777 (2021). https://doi.org/10.1016/j.neulet.2021.135777
36 Association, A. P. *Diagnostic and statistical manual of mental disorders*. 5th ed., text rev edn, (2022).
37 Kessler, R. C. *et al.* Anxious and non-anxious major depressive disorder in the World Health Organization World Mental Health Surveys. *Epidemiol Psychiatr Sci* **24**, 210-226 (2015). https://doi.org/10.1017/S2045796015000189
38 Roybal, K. *et al.* Mania-like behavior induced by disruption of CLOCK. *Proc Natl Acad Sci U S A* **104**, 6406-6411 (2007).
39 King, D. P. *et al.* Positional cloning of the mouse circadian clock gene. *Cell* **89**, 641-653 (1997).
40 Dzirasa, K. *et al.* Lithium ameliorates nucleus accumbens phase signaling dysfunction in a genetic mouse model of mania. *J Neurosci* **30**, 16314 –16323 (2010).
41 Logan, R. W. *et al.* Valproate reverses mania-like behaviors in mice via preferential targeting of HDAC2. *Mol Psychiatry* **26**, 4066-4084 (2021). https://doi.org/10.1038/s41380-020-00958-2
42 Krishnan, V. *et al.* Molecular adaptations underlying susceptibility and resistance to social defeat in brain reward regions. *Cell* **131**, 391-404 (2007).

43 Berton, O. *et al.* Essential role of BDNF in the mesolimbic dopamine pathway in social defeat stress. *Science* **311**, 864-868 (2006).
44 Morel, C. *et al.* Midbrain projection to the basolateral amygdala encodes anxiety-like but not depression-like behaviors. *Nat Commun* **13**, 1532 (2022). https://doi.org/10.1038/s41467-022-29155-1
45 Zhong, P. *et al.* HCN2 channels in the ventral tegmental area regulate behavioral responses to chronic stress. *Elife* **7** (2018). https://doi.org/10.7554/eLife.32420
46 Monteiro, S. *et al.* An efficient chronic unpredictable stress protocol to induce stress-related responses in C57BL/6 mice. *Front Psychiatry* **6**, 6 (2015). https://doi.org/10.3389/fpsyt.2015.00006
47 Golden, S. A., Covington, H. E., 3rd, Berton, O. & Russo, S. J. A standardized protocol for repeated social defeat stress in mice. *Nature protocols* **6**, 1183-1191 (2011). https://doi.org/10.1038/nprot.2011.361
48 Tsankova, N. M. *et al.* Sustained hippocampal chromatin regulation in a mouse model of depression and antidepressant action. *Nat Neurosci* **9**, 519-525 (2006). https://doi.org/10.1038/nn1659
49 Dzirasa, K., Fuentes, R., Kumar, S., Potes, J. M. & Nicolelis, M. A. Chronic in vivo multi-circuit neurophysiological recordings in mice. *Journal of neuroscience methods* **195**, 36-46 (2011). https://doi.org/10.1016/j.jneumeth.2010.11.014
50 Carlson, D. *et al.* Dynamically Timed Stimulation of Corticolimbic Circuitry Activates a Stress-Compensatory Pathway. *Biol Psychiatry* **82**, 904-913 (2017). https://doi.org/10.1016/j.biopsych.2017.06.008
51 Grossman, Y. *et al.* A widespead oscillatory network encodes an aggressive internal state. *BioRxiv* (2024). https://doi.org/https://doi.org/10.1101/2022.12.07.519272
52 Geweke, J. Measurement of Linear Dependence and Feedback between Multiple Time Series. . *Journal of the American Statistical Association* **77**, 304–313 (1982).
53 Barnett, L. & Seth, A. K. The MVGC multivariate Granger causality toolbox: a new approach to Granger-causal inference. *Journal of neuroscience methods* **223**, 50-68 (2014). https://doi.org/10.1016/j.jneumeth.2013.10.018
54 Crawley, J. N. *What's Wrong With My Mouse?: behavioral phenotyping of transgenic and knockout mice*. Second edn, (John Wiley & Sons, Inc., 2007).
55 Dzirasa, K. *et al.* Dopaminergic control of sleep-wake states. *J Neurosci* **26**, 10577-10589 (2006). https://doi.org/10.1523/JNEUROSCI.1767-06.2006
56 Sweis, B. M. *et al.* Sensitivity to "sunk costs" in mice, rats, and humans. *Science* **361**, 178-181 (2018). https://doi.org/10.1126/science.aar8644
57 Durand-de Cuttoli, R. *et al.* Distinct forms of regret linked to resilience versus susceptibility to stress are regulated by region-specific CREB function in mice. *Sci Adv* **8**, eadd5579 (2022). https://doi.org/10.1126/sciadv.add5579
58 Kumar, S. *et al.* Cortical Control of Affective Networks. *J Neurosci* **33**, 1116 –1129 (2013).
59 Hultman, R. *et al.* Dysregulation of Prefrontal Cortex-Mediated Slow-Evolving Limbic Dynamics Drives Stress-Induced Emotional Pathology. *Neuron* **91**, 439-452 (2016). https://doi.org/10.1016/j.neuron.2016.05.038
60 Mathis, A. *et al.* DeepLabCut: markerless pose estimation of user-defined body parts with deep learning. *Nat Neurosci* **21**, 1281-1289 (2018). https://doi.org/10.1038/s41593-018-0209-y
61 Kumar, S. *et al.* Prefrontal cortex reactivity underlies trait vulnerability to chronic social defeat stress. *Nat Commun* **5**, 4537 (2014). https://doi.org/10.1038/ncomms5537
62 Carlson, D. E., Chavarriaga, R., Liu, Y., Lotte, F. & Lu, B. L. The NERVE-ML (neural engineering reproducibility and validity essentials for machine learning) checklist: ensuring machine learning

advances neural engineering(). *J Neural Eng* **22** (2025). https://doi.org/10.1088/1741-2552/adbfbd

63 Carson, W. E. t. *et al.* Model selection to achieve reproducible associations between resting state EEG features and autism. *Scientific reports* **14**, 25301 (2024). https://doi.org/10.1038/s41598-024-76659-5

64 Kuhn, H. W. The Hungarian method for the assignment problem. *Naval Research Logistics Quarterly* **2**, 83-97 (1955). https://doi.org/https://doi.org/10.1002/nav.3800020109

65 Zhou, P. *et al.* Towards theoretically understanding why SGD generalizes better than ADAM in deep learning. *Proceedings of the 34th International Conference on Neural Information Processing Systems* **20**, 21285–21296 (2020).

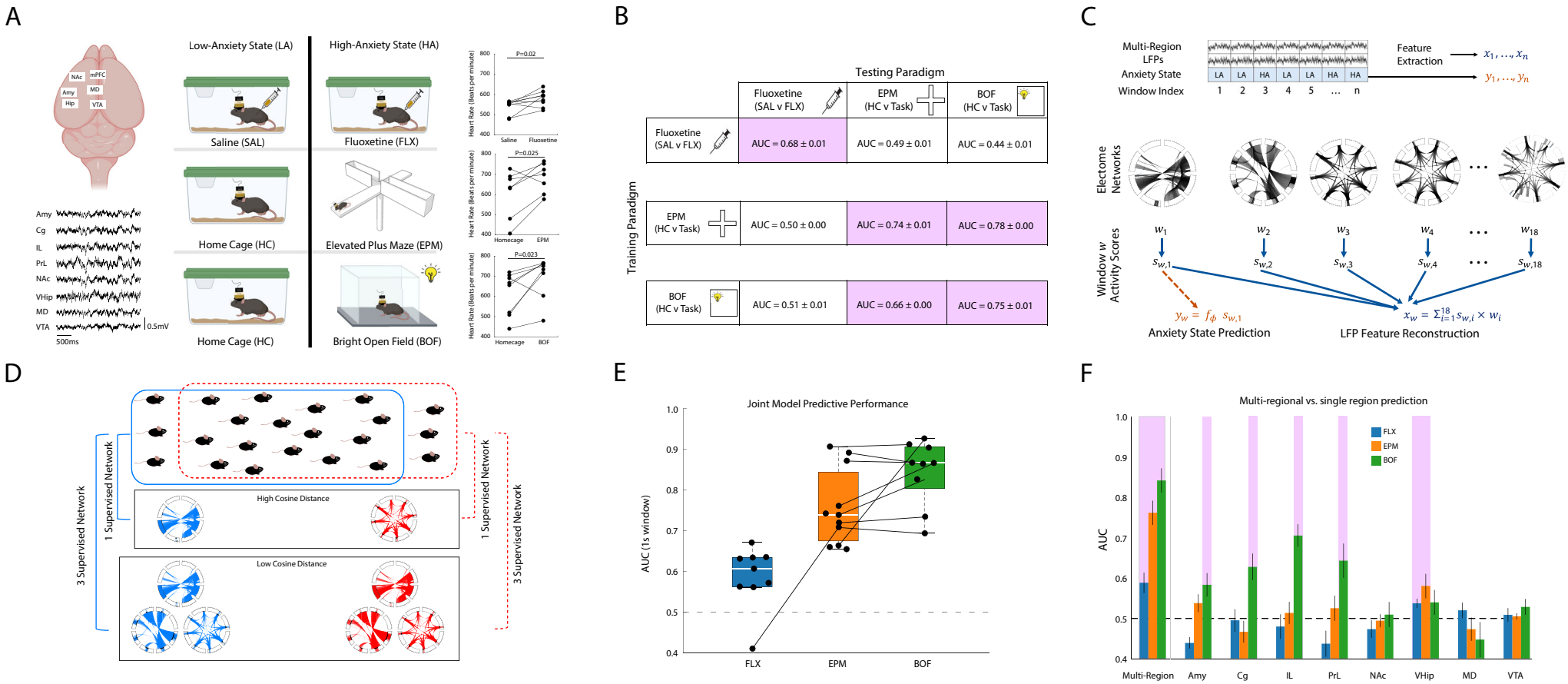
A
Low-Anxiety State (LA)
High-Anxiety State (HA)
NAc
mPFC
Amy
MD
Hip
VTA
Saline (SAL)
Fluoxetine (FLX)
Home Cage (HC)
Elevated Plus Maze (EPM)
Home Cage (HC)
Bright Open Field (BOF)
Amy
Cg
IL
PrL
NAc
VHip
MD
VTA
0.5mV
500ms
P=0.02
P=0.025
P=0.023
Heart Rate (Beats per minute)
Saline
Fluoxetine
Homecage
EPM
BOF
B
Testing Paradigm
Training Paradigm
Fluoxetine (SAL v FLX)
EPM (HC v Task)
BOF (HC v Task)
AUC = 0.68 ± 0.01
AUC = 0.49 ± 0.01
AUC = 0.44 ± 0.01
AUC = 0.50 ± 0.00
AUC = 0.74 ± 0.01
AUC = 0.78 ± 0.00
AUC = 0.51 ± 0.01
AUC = 0.66 ± 0.00
AUC = 0.75 ± 0.01
C
Multi-Region LFPs
Anxiety State
Window Index
LA LA HA LA LA HA HA
1 2 3 4 5 … n
Feature Extraction
$x_1, \ldots, x_n$
$y_1, \ldots, y_n$
Electome Networks
Window w Activity Scores
w_1 w_2 w_3 w_4 … w_{18}
$s_{w,1}$ $s_{w,2}$ $s_{w,3}$ $s_{w,4}$ … $s_{w,18}$
$y_w = f_\phi \; s_{w,1}$
$x_w = \Sigma_{i=1}^{18} s_{w,i} \times w_i$
Anxiety State Prediction
LFP Feature Reconstruction
D
3 Supervised Network
1 Supervised Network
High Cosine Distance
Low Cosine Distance
1 Supervised Network
3 Supervised Network
E
Joint Model Predictive Performance
AUC (1s window)
FLX
EPM
BOF
F
Multi-regional vs. single region prediction
AUC
FLX
EPM
BOF
Multi-Region
Amy
Cg
IL
PrL
NAc
VHip
MD
VTA

Figure 1

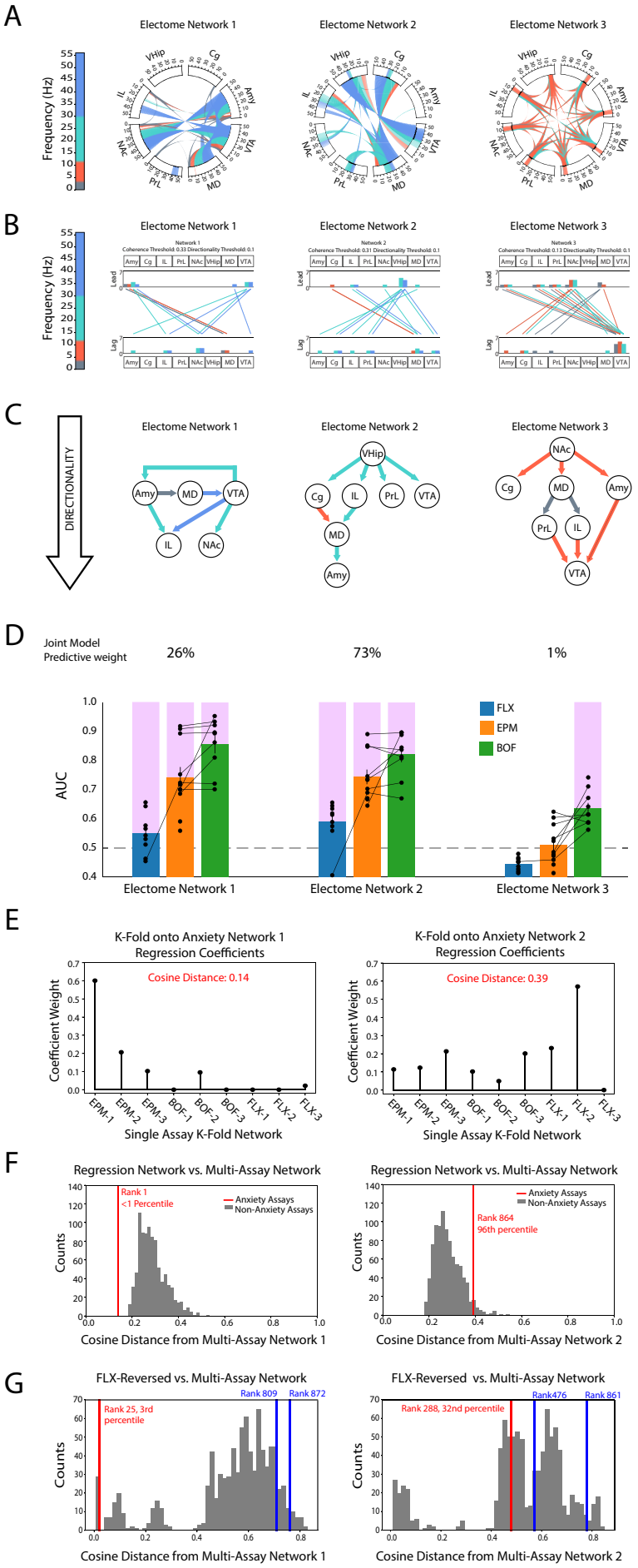
A
Electome Network 1
Electome Network 2
Electome Network 3
Frequency (Hz)
VHip
Cg
Amy
VTA
MD
PrL
NAc
IL
B
Electome Network 1
Electome Network 2
Electome Network 3
Frequency (Hz)
Lead
Lag
C
DIRECTIONALITY
Electome Network 1
Electome Network 2
Electome Network 3
D
Joint Model
Predictive weight
26%
73%
1%
AUC
FLX
EPM
BOF
Electome Network 1
Electome Network 2
Electome Network 3
E
K-Fold onto Anxiety Network 1
Regression Coefficients
Cosine Distance: 0.14
Coefficient Weight
Single Assay K-Fold Network
K-Fold onto Anxiety Network 2
Regression Coefficients
Cosine Distance: 0.39
Coefficient Weight
Single Assay K-Fold Network
F
Regression Network vs. Multi-Assay Network
Rank 1
<1 Percentile
Anxiety Assays
Non-Anxiety Assays
Counts
Cosine Distance from Multi-Assay Network 1
Regression Network vs. Multi-Assay Network
Anxiety Assays
Non-Anxiety Assays
Rank 864
96th percentile
Counts
Cosine Distance from Multi-Assay Network 2
G
FLX-Reversed vs. Multi-Assay Network
Rank 809
Rank 872
Rank 25, 3rd
percentile
Counts
Cosine Distance from Multi-Assay Network 1
FLX-Reversed vs. Multi-Assay Network
Rank476
Rank 861
Rank 288, 32nd percentile
Counts
Cosine Distance from Multi-Assay Network 2

Figure 2

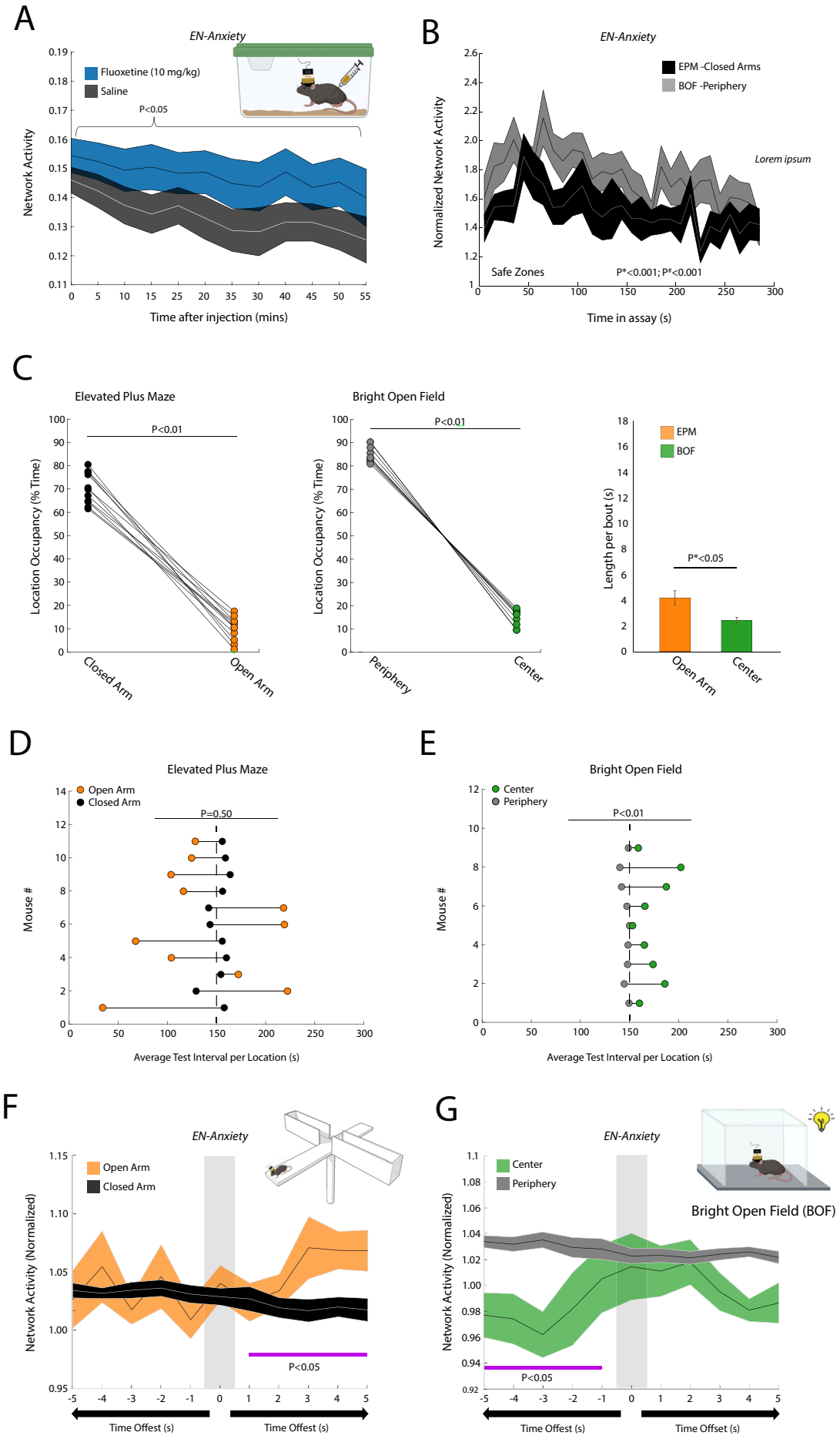
A
EN-Anxiety
Fluoxetine (10 mg/kg)
Saline
P<0.05
Network Activity
Time after injection (mins)
B
EN-Anxiety
EPM -Closed Arms
BOF -Periphery
Lorem ipsum
Safe Zones
P*<0.001; P*<0.001
Normalized Network Activity
Time in assay (s)
C
Elevated Plus Maze
P<0.01
Location Occupancy (% Time)
Closed Arm
Open Arm
Bright Open Field
P<0.01
Location Occupancy (% Time)
Periphery
Center
EPM
BOF
P*<0.05
Length per bout (s)
Open Arm
Center
D
Elevated Plus Maze
Open Arm
Closed Arm
P=0.50
Mouse #
Average Test Interval per Location (s)
E
Bright Open Field
Center
Periphery
P<0.01
Mouse #
Average Test Interval per Location (s)
F
EN-Anxiety
Open Arm
Closed Arm
P<0.05
Network Activity (Normalized)
Time Offest (s)
Time Offest (s)
G
EN-Anxiety
Center
Periphery
Bright Open Field (BOF)
P<0.05
Network Activity (Normalized)
Time Offest (s)
Time Offset (s)

Figure 3

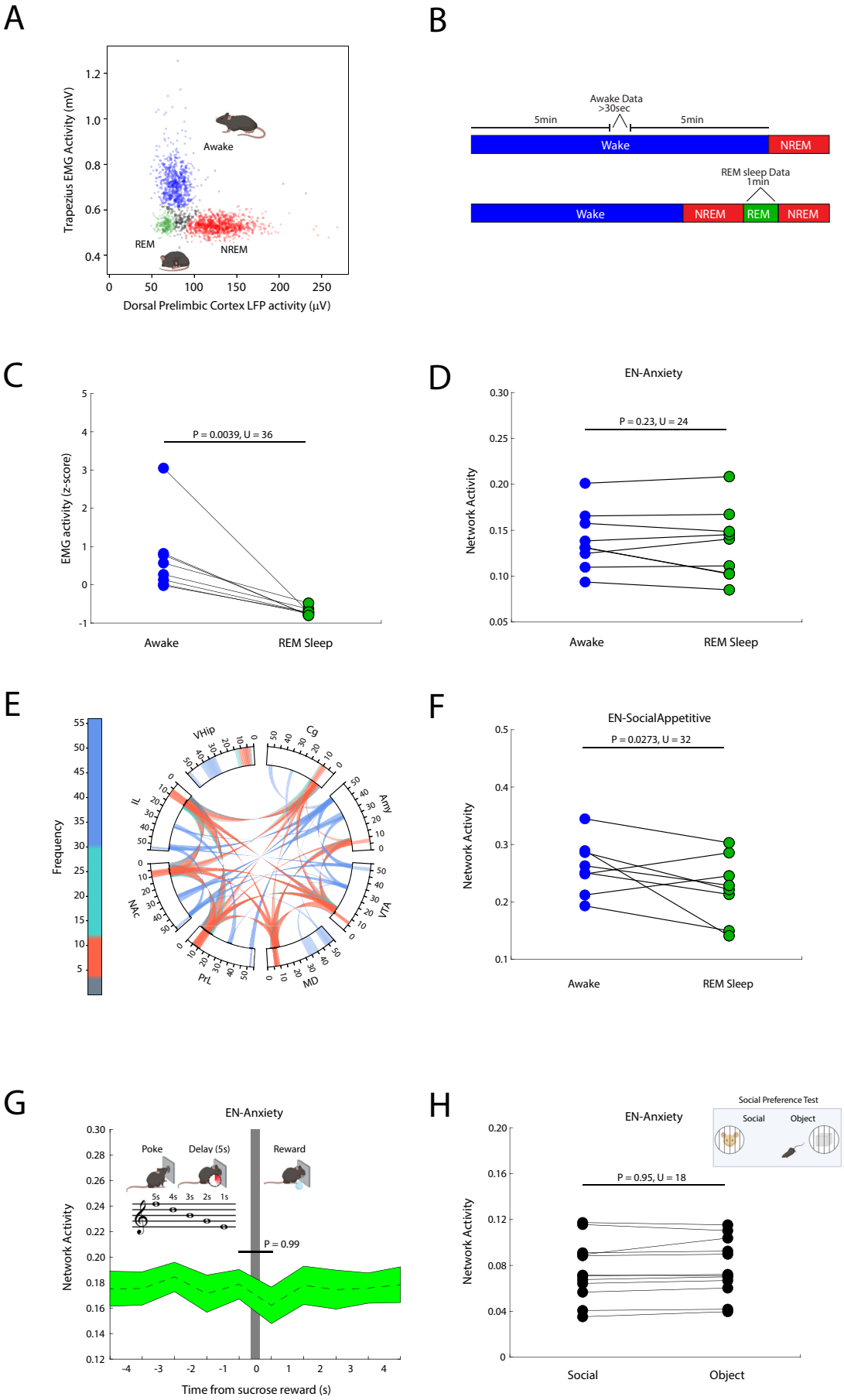
A
Trapezius EMG Activity (mV)
Dorsal Prelimbic Cortex LFP activity (µV)
Awake
REM
NREM
B
Awake Data
>30sec
5min
5min
Wake
NREM
REM sleep Data
1min
Wake
NREM
REM
NREM
C
EMG activity (z-score)
P = 0.0039, U = 36
Awake
REM Sleep
D
EN-Anxiety
Network Activity
P = 0.23, U = 24
Awake
REM Sleep
E
Frequency
VHip
Cg
Amy
VTA
MD
PrL
NAc
IL
F
EN-SocialAppetitive
Network Activity
P = 0.0273, U = 32
Awake
REM Sleep
G
EN-Anxiety
Poke
Delay (5s)
Reward
5s 4s 3s 2s 1s
P = 0.99
Network Activity
Time from sucrose reward (s)
H
EN-Anxiety
Social Preference Test
Social
Object
P = 0.95, U = 18
Network Activity
Social
Object

Figure 4

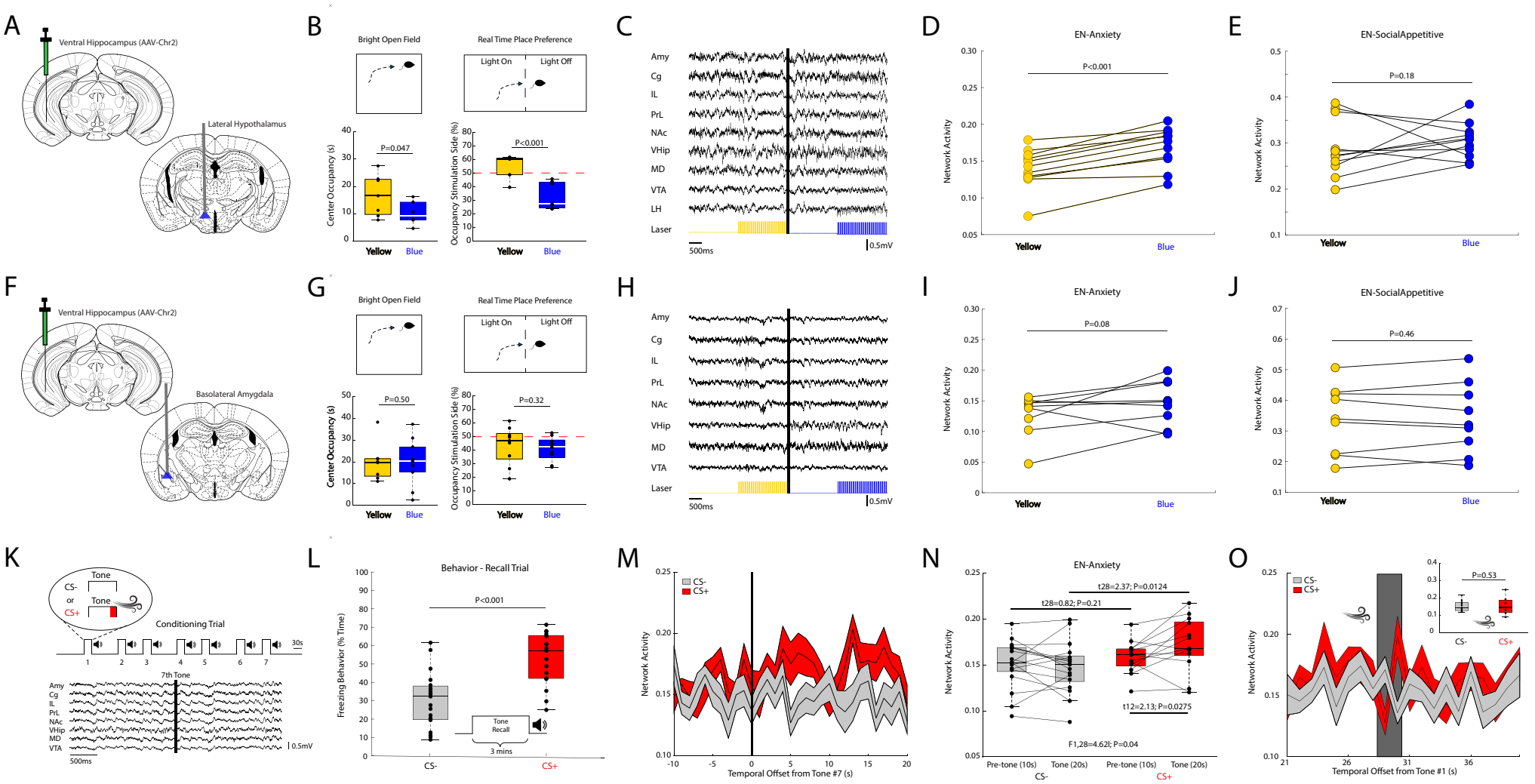
A
Ventral Hippocampus (AAV-Chr2)
Lateral Hypothalamus
B
Bright Open Field
Real Time Place Preference
Light On
Light Off
Center Occupancy (s)
P=0.047
Occupancy Stimulation Side (%)
P<0.001
Yellow
Blue
C
Amy
Cg
IL
PrL
NAc
VHip
MD
VTA
LH
Laser
500ms
0.5mV
D
EN-Anxiety
P<0.001
Network Activity
Yellow
Blue
E
EN-SocialAppetitive
P=0.18
Network Activity
Yellow
Blue
F
Ventral Hippocampus (AAV-Chr2)
Basolateral Amygdala
G
Bright Open Field
Real Time Place Preference
Light On
Light Off
Center Occupancy (s)
P=0.50
Occupancy Stimulation Side (%)
P=0.32
Yellow
Blue
H
Amy
Cg
IL
PrL
NAc
VHip
MD
VTA
Laser
500ms
0.5mV
I
EN-Anxiety
P=0.08
Network Activity
Yellow
Blue
J
EN-SocialAppetitive
P=0.46
Network Activity
Yellow
Blue
K
Tone
CS-
or
Tone
CS+
Conditioning Trial
30s
7th Tone
Amy
Cg
IL
PrL
NAc
VHip
MD
VTA
500ms
0.5mV
L
Behavior - Recall Trial
P<0.001
Freezing Behavior (% Time)
Tone Recall
3 mins
CS-
CS+
M
CS-
CS+
Network Activity
Temporal Offset from Tone #7 (s)
N
EN-Anxiety
t28=2.37; P=0.0124
t28=0.82; P=0.21
t12=2.13; P=0.0275
F1,28=4.62l; P=0.04
Network Activity
Pre-tone (10s)
Tone (20s)
Pre-tone (10s)
Tone (20s)
CS-
CS+
O
CS-
CS+
P=0.53
Network Activity
Temporal Offset from Tone #1 (s)

Figure 5

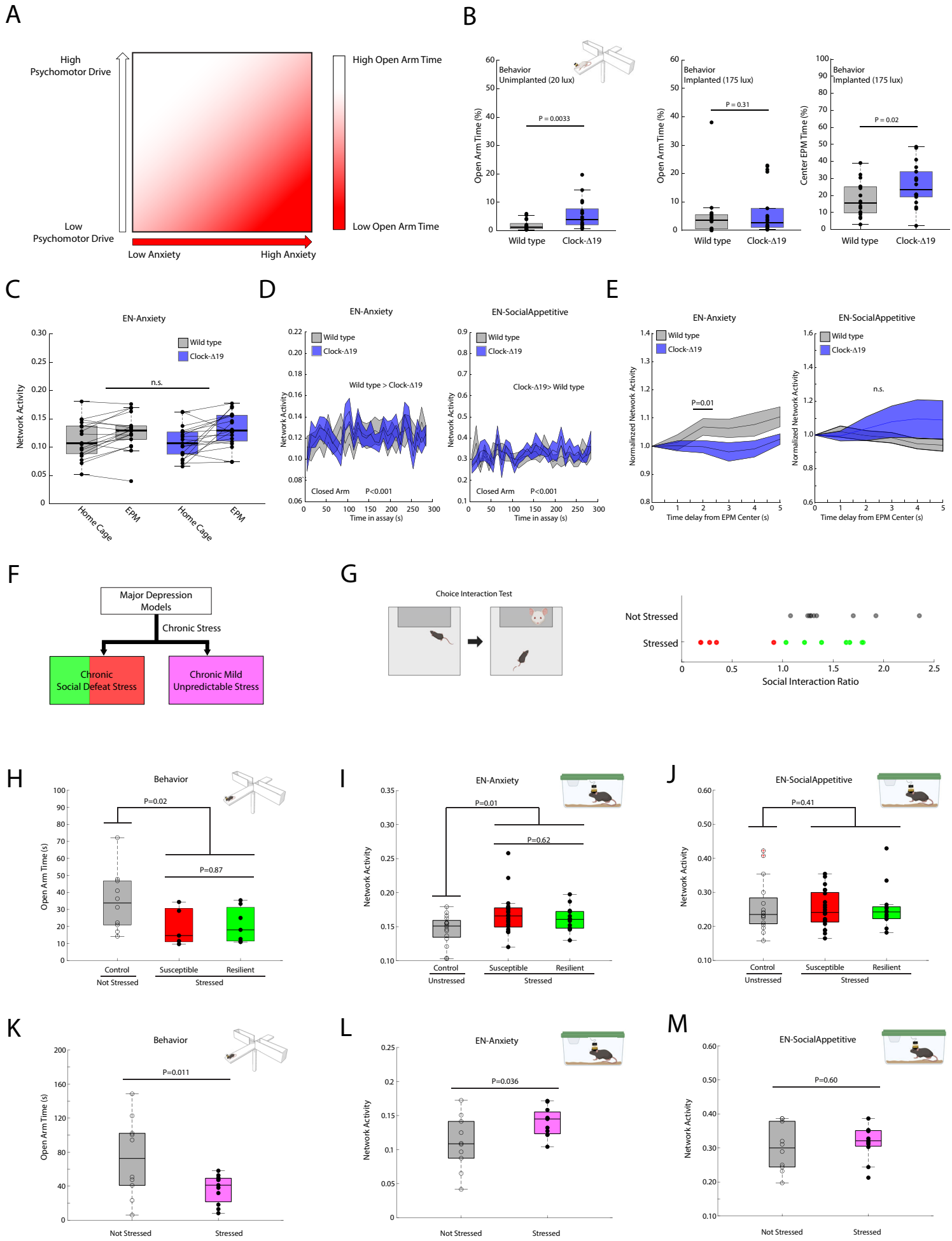
A
High Psychomotor Drive
Low Psychomotor Drive
Low Anxiety
High Anxiety
High Open Arm Time
Low Open Arm Time
B
Behavior Unimplanted (20 lux)
P = 0.0033
Open Arm Time (%)
Wild type
Clock-Δ19
Behavior Implanted (175 lux)
P = 0.31
Behavior Implanted (175 lux)
P = 0.02
Center EPM Time (%)
C
EN-Anxiety
Wild type
Clock-Δ19
n.s.
Network Activity
Home Cage
EPM
D
EN-Anxiety
Wild type > Clock-Δ19
Closed Arm
P<0.001
Time in assay (s)
EN-SocialAppetitive
Clock-Δ19> Wild type
E
EN-Anxiety
P=0.01
Normalized Network Activity
Time delay from EPM Center (s)
EN-SocialAppetitive
n.s.
F
Major Depression Models
Chronic Stress
Chronic Social Defeat Stress
Chronic Mild Unpredictable Stress
G
Choice Interaction Test
Not Stressed
Stressed
Social Interaction Ratio
H
Behavior
P=0.02
P=0.87
Open Arm Time (s)
Control
Susceptible
Resilient
Not Stressed
Stressed
I
EN-Anxiety
P=0.01
P=0.62
Network Activity
Unstressed
J
EN-SocialAppetitive
P=0.41
K
Behavior
P=0.011
L
EN-Anxiety
P=0.036
M
EN-SocialAppetitive
P=0.60

Figure 6

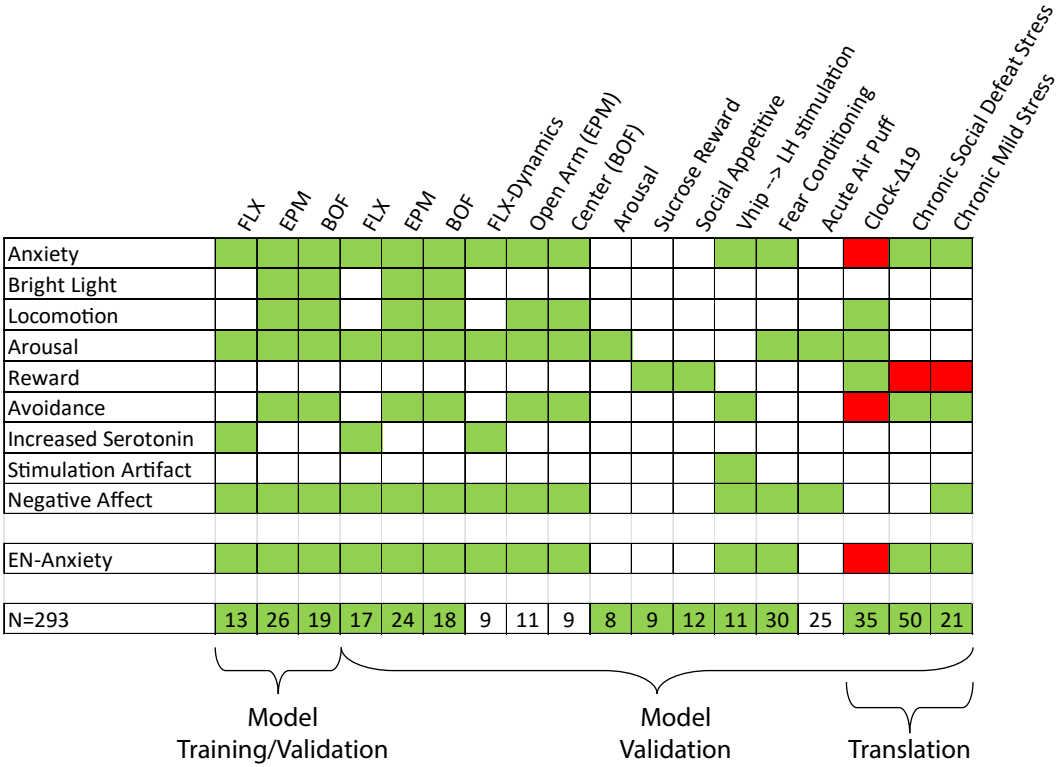
FLX
EPM
BOF
FLX
EPM
BOF
FLX-Dynamics
Open Arm (EPM)
Center (BOF)
Arousal
Sucrose Reward
Social Appetitive
Vhip --> LH stimulation
Fear Conditioning
Acute Air Puff
Clock-Δ19
Chronic Social Defeat Stress
Chronic Mild Stress
Anxiety
Bright Light
Locomotion
Arousal
Reward
Avoidance
Increased Serotonin
Stimulation Artifact
Negative Affect
EN-Anxiety
N=293
13 26 19 17 24 18 9 11 9 8 9 12 11 30 25 35 50 21
Model Training/Validation
Model Validation
Translation

Figure 7